Inorganic Chemistry

Article

pubs.acs.org/IC

Utilization of Phosphinoamide Ligands in Homobimetallic Fe and Mn Complexes: The Effect of Disparate Coordination Environments on Metal–Metal Interactions and Magnetic and Redox Properties

Subramaniam Kuppuswamy,[†] Mark W. Bezpalko,[†] Tamara M. Powers,[§] Mark M. Turnbull,[‡] Bruce M. Foxman,[†] and Christine M. Thomas*[,†]

[†]Department of Chemistry, Brandeis University, 415 South Street, Waltham, Massachusetts 02454, United States

[‡]Carlson School of Chemistry and Biochemistry, Clark University, 950 Main Street, Worcester, Massachusetts 01610, United States

[§]Department of Chemistry and Chemical Biology, Harvard University, Cambridge, Massachusetts 02139, United States

Supporting Information

ABSTRACT: A series of homobimetallic phosphinoamide-bridged diiron and dimanganese complexes in which the two metals maintain different coordination environments have been synthesized. Systematic variation of the steric and electronic properties of the phosphinoamide phosphorus and nitrogen substituents leads to structurally different complexes. Reaction of [^{i}PrNKPPh$_2$] (**1**) with MCl$_2$ (M = Mn, Fe) affords the phosphinoamide-bridged bimetallic complexes [Mn(^{i}PrNPPh$_2$)$_3$Mn(^{i}PrNPPh$_2$)] (**3**) and [Fe(^{i}PrNPPh$_2$)$_3$Fe(^{i}PrNPPh$_2$)] (**4**). Complexes **3** and **4** are iso-structural, with one metal center preferentially binding to the three amide ligands in a trigonal planar arrangement while the second metal center is ligated by three phosphine donors. A fourth phosphinoamide ligand caps the tetrahedral coordination sphere of the phosphine-ligated metal center. Mössbauer spectroscopy of complex **4** suggests that the metals in these complexes are best described as Fe^{II} centers. In contrast, treatment of MnCl$_2$ or FeI$_2$ with [MesNKP^{i}Pr$_2$] (**2**) leads to the formation of the halide-bridged species [(THF)Mn(μ-Cl)(MesNP^{i}Pr$_2$)$_2$Mn(MesNP^{i}Pr$_2$)] (**5**) and [(THF)Fe(μ-I)(MesNP^{i}Pr$_2$)$_2$FeI (**7**), respectively. Utilization of FeCl$_2$ in place of FeI$_2$, however, leads exclusively to the C$_3$-symmetric complex [Fe(MesNP^{i}Pr$_2$)$_3$FeCl] (**6**), structurally similar to **4** but with a halide bound to the phosphine-ligated Fe center. The Mössbauer spectrum of **6** is also consistent with high spin Fe^{II} centers. Thus, in the case of the [^{i}PrNPPh$_2$]$^-$ and [MesNP^{i}Pr$_2$]$^-$ ligands, zwitterionic complexes with the two metals in disparate coordination environments are preferentially formed. In the case of the more electron-rich ligand [^{i}PrNP^{i}Pr$_2$]$^-$, complexes with a 2:1 mixed donor ligand arrangement, in which one of the ligand arms has reversed orientation relative to the previous examples, are formed exclusively when [^{i}PrNLiP^{i}Pr$_2$] (generated in situ) is treated with MCl$_2$ (M = Mn, Fe): (THF)$_3$LiCl[Mn(N^{i}PrP^{i}Pr$_2$)$_2$(P^{i}Pr$_2$N^{i}Pr)MnCl] (**8**) and [Fe(N^{i}PrP^{i}Pr$_2$)$_2$(P^{i}Pr$_2$N^{i}Pr)FeCl] (**9**). Bimetallic complexes **3**–**9** have been structurally characterized using X-ray crystallography, revealing Fe–Fe interatomic distances indicative of metal–metal bonding in complexes **6** and **9** (and perhaps **4**, to a lesser extent). All of the complexes appear to adopt high spin electron configurations, and magnetic measurements indicate significant antiferromagnetic interactions in Mn$_2$ complexes **5** and **8** and no discernible magnetic superexchange in Fe$_2$ complex **4**. The redox behavior of complexes **3**–**9** has also been investigated using cyclic voltammetry, and theoretical investigations (DFT) were performed to gain insight into the metal–metal interactions in these unique asymmetric complexes.

INTRODUCTION

Multimetallic transition metal complexes have received considerable attention in recent years owing to their ability to facilitate multielectron redox processes, their potential applications in catalysis, and their parallels to enzymatic active sites.[1] Of particular importance is the electronic communication between multiple metal centers and the resulting effects on electronic structure. Recent contributions in this area include elegant multidentate ligand designs capable of supporting well-defined trinuclear complexes.[2−5] The interplay between the metal centers in these compounds gives rise to multielectron redox chemistry and unique magnetic properties,[4,6,7] and in some cases provides an intriguing model of complex enzymatic active sites.[8] Dinuclear active sites featuring two late transition metals are also prevalent in metalloenzymes, including carbon monoxide dehydrogenases,[9,10] acetyl-coenzymeA synthase,[9,10] heme-copper oxidases,[11] dimanganese enzymes,[12] methane monooxgyenases,[13,14] and hydrogenases.[15,16] Metal–metal interactions in symmetric homobimetallic complexes of second

Received: April 14, 2012
Published: July 17, 2012

   dx.doi.org/10.1021/ic300776y | Inorg. Chem. 2012, 51, 8225–8240

and third row transition metals have been investigated extensively, most notably in the 4-fold symmetric metal−metal multiple bonding regime.[17−19] Metal−metal bonds in high spin dinuclear complexes of the first transition series, however, remain quite rare and are understood to a far lesser extent.

Many groups have been interested in heterobimetallic combinations of early and late transition metal fragments, as the unusually polar metal−metal interactions and different Lewis acid/base properties of the two component metal centers are likely to lead to new and interesting reactivity patterns.[20−24] Our group, in particular, has recently focused on such early/late metal combinations linked by phosphinoamide ligands, utilizing the hard/soft acid/base properties of the phosphine and amide donors to preferentially coordinate late and early metals, respectively.[25] The metal−metal interactions in early/late heterobimetallic complexes of this type have been shown to have a drastic effect on redox potentials and lead to interesting reactivity toward small molecule substrates (e.g., alkyl halides, H_2, CO_2).[26−30]

Using what we have learned from phosphinoamide-linked early/late heterobimetallic systems, we have begun to investigate homodinuclear systems in which the metals are in coordination environments that differ substantially in terms of hard (amide) and soft (phosphine) donor functionalities. Little research has been done in the area of homobimetallic complexes featuring metals in disparate coordination environments. While a large number of dinuclear late transition metal complexes have been reported, these are typically formed using bridging ligands that present similar (hard/hard or soft/soft) donors to each metal and, thus, lead to metals in similar electronic environments.[31,32] An interesting class of polynuclear metal clusters composed of metal−metal interactions between one hard open-shell metal and a second soft metal typically supported by carbonyls has recently emerged in the literature.[33,34] Theoretical investigations of these "xenophilic" complexes have suggested that the disparate coordination environments on two appended late transition metals may lead to unusual electronic properties and magnetic behavior.[35] In particular, we are curious whether different electronic environments about two similar metal centers are enough to promote dative metal−metal interactions. A recent theory posed by Lindahl suggests that such metal−metal interactions may play a role in the catalytic mechanism of a number of bimetallic enzyme active sites.[36] Moreover, differentiating the two metal centers in bimetallic compounds via their coordination spheres may prove a useful method for promoting two-electron mixed valence.[32]

Several high spin dinuclear Fe complexes have been reported, and the electronic structure and metal−metal bonding within these compounds appears highly variable.[37−41] Notably, the high spin nature of the Fe centers in these complexes results in unusually high spin states (as high as $S = 4$) in combination with strong metal−metal interactions. The 3-fold symmetric "trigonal lantern" complex $Fe_2(DPhF)_3$ (DPhF = diphenylformamidinate) presents an archetypical example of metal−metal multiple bonding in a high spin complex, with an extremely short Fe−Fe bond distance (2.2318(8) Å) and an $S = 7/2$ ground state.[40] Cotton and co-workers provided a preliminary explanation for the nature of the metal−metal bonding in $Fe_2(DPhF)_3$,[42] and Lu and co-workers recently revisited this rare example of a ferromagnetically coupled metal−metal bonded compound using advanced computational and spectroscopic methods.[43] The electronic structure of a similar 4-fold symmetric formamidinate complex $Fe_2(DPhF)_4$[44] has also been investigated computationally by Berry and co-workers.[45] In contrast to iron systems, high spin polynuclear manganese complexes tend to exhibit antiferromagnetic coupling and weaker metal−metal interactions.[2,46−50]

To date, all of the reported non-organometallic metal−metal bonded first row transition metal complexes in the literature are supported by symmetric ligand sets that present identical donors to both Fe centers, providing a high degree of delocalization. Herein, we present the first examples of high spin diiron and dimanganese complexes in which the metal sites are coordinated by distinctly different ligand sets. Phosphinoamide ligands of the type $[R_2PNR']^-$ are utilized, as an extension of our earlier work with heterobimetallic compounds.[25,51] In contrast to other P,N-binucleating ligands in the literature that tend to have softer N-donors such as amines or pyridines, phosphinoamides present one hard and one soft ligand donor, leading to metal centers whose coordination spheres are substantially different.[31] In the context of homobimetallic complexes, phosphinoamide ligands have been reported to stabilize homodinuclear Ni^{II} and Pd^{II} complexes,[52] as well as Cr^{II} complexes with activities toward ethylene oligomerization.[53] We now extend this chemistry to Mn^{II} and Fe^{II}, utilizing three different phosphinoamide linkers, and analyze the complex electronic and magnetic properties of these new compounds.

RESULTS AND DISCUSSION

Synthesis and Characterization of 1−9. Salt metathesis reactions are a convenient route for the preparation of late transition metal amides under mild conditions. Treatment of the phosphinoamines ^{i}PrNHPPh$_2$ and MesNHP^{i}Pr$_2$ with 1.02 equiv of KH at room temperature in tetrahydrofuran (THF) affords [^{i}PrNKPPh$_2$] (**1**) and [MesNKP^{i}Pr$_2$] (**2**) as air and moisture sensitive yellow or colorless crystalline solids, respectively (Scheme 1). Characteristic ^{31}P NMR resonances

Scheme 1

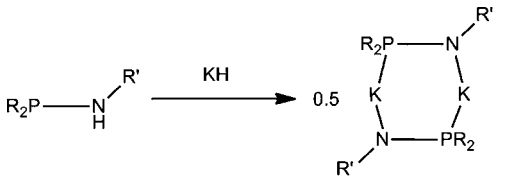

R = Ph, R' = ^{i}Pr (**1**)
R = ^{i}Pr, R' = Mes (**2**)

centered at 46.2 ppm (**1**) and 72.3 ppm (**2**) are observed significantly downfield compared to the protonated ligands (35 and 57 ppm, respectively). The dimeric structures of **1** and **2** are inferred based on analogy to the structurally characterized lithium phosphinoamides previously reported.[54]

Potassium amides **1** and **2** are excellent precursors for the preparation of late transition metal phosphinoamide complexes: Salt methathesis of **1** with MCl_2 (M = Mn or Fe) at ambient temperature leads to the formation of [Mn(^{i}PrNPPh$_2$)$_3$Mn(^{i}PrNPPh$_2$)] (**3**) and [Fe(^{i}PrNPPh$_2$)$_3$Fe(^{i}PrNPPh$_2$)] (**4**) as yellow and purple crystalline solids, respectively (Scheme 2). The ^{1}H NMR of complex **3** features two broad unresolvable resonances, as is typical for high spin Mn complexes, but the analytical purity of **3** is nonetheless confirmed by combustion

dx.doi.org/10.1021/ic300776y | Inorg. Chem. 2012, 51, 8225−8240

Scheme 2

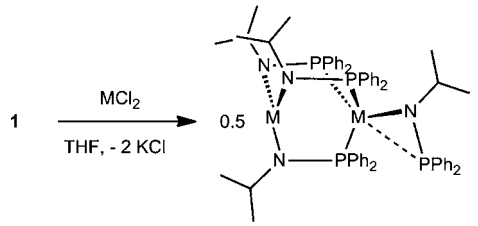

M = Mn, **3**; Fe, **4**

analysis. On the other hand, the analogous iron complex **4** has an informative ^{1}H NMR spectrum that exhibits 10 paramagnetically shifted broad resonances between +51 and −31 ppm, indicative of two inequivalent phosphinoamide environments. On the basis of the number of ^{1}H NMR resonances and their relative intensities, complex **4** was tentatively assigned as having three bridging phosphinoamide ligands, with one additional terminal phosphinoamide (later confirmed crystallographically, vide infra).

Investigating a phosphinoamide ligand set with different steric and electronic properties led to structurally different homobimetallic species. Metathesis of [MesNKP^{i}Pr$_2$] (**2**) and $MnCl_2$ results in formation of [(THF)Mn(μ-Cl)-(MesNP^{i}Pr$_2$)$_2$Mn(MesNP^{i}Pr$_2$)] (**5**) as a reddish yellow crystalline solid in 40% yield (Scheme 3). Again, the ^{1}H NMR spectrum of high spin Mn complex **5** is uninformative, exhibiting only two broad and featureless resonances. The exact formulation and connectivity of **5** could only be determined crystallographically (vide infra). In the case of Fe, treatment of [MesNKP^{i}Pr$_2$] (**2**) with $FeCl_2$ provides [Fe(MesNP^{i}Pr$_2$)$_3$FeCl] (**6**) as an analytically pure pale yellow crystalline solid in 70%

Scheme 3

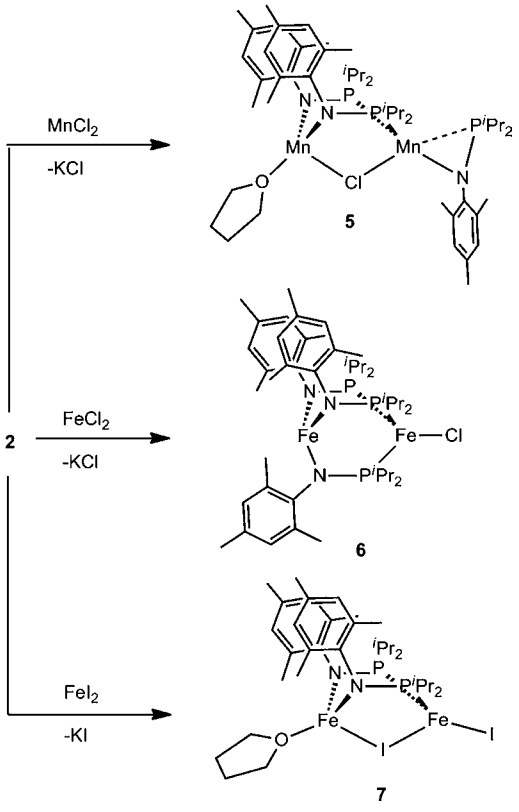

yield. Conversely, the reaction between [MesNKP^{i}Pr$_2$] (**2**) and FeI_2 affords [(THF)Fe(μ-I)(MesNP^{i}Pr$_2$)$_2$FeI] (**7**) as a brown crystalline solid in 50% yield. The resonances in the ^{1}H NMR spectrum of **6** and **7** appear over a 50 ppm chemical shift window, but are nonetheless interpretable. The ^{1}H NMR spectrum of **6** shows 6 very broad resonances between +44 and +1 ppm, indicative of a C_3-symmetric ligand environment without an additional terminal phosphinoamide ligand. Eleven broad paramagnetic resonances are observed between +59 and −16 ppm in the ^{1}H NMR of complex **7**, corresponding to a C_s-symmetric molecule with two signals for the coordinated THF ligand.

Attempts to isolate alkali metal salts of the electron rich phosphinoamine ^{i}PrNHP^{i}Pr$_2$ failed under various reaction conditions owing to the solubilizing isopropyl substituents. Therefore, the lithium amide [^{i}PrNLiP^{i}Pr$_2$] was generated in situ via treatment of an equimolar ratio of ^{i}PrNHP^{i}Pr$_2$ with ^{n}BuLi. Subsequent addition of $MnCl_2$ in THF affords an amber red crystalline solid identified as (THF)$_3$LiCl[Mn(N^{i}PrP^{i}Pr$_2$)$_2$(P^{i}Pr$_2$N^{i}Pr)MnCl] (**8**) in 56% yield (Scheme 4).

Scheme 4

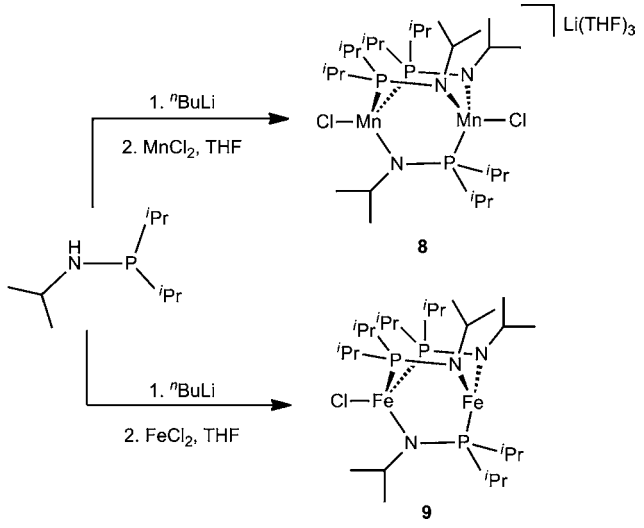

Once again, the ^{1}H NMR spectrum of **8** shows two broad featureless peaks that are not readily assigned. Complex [Fe(N^{i}PrP^{i}Pr$_2$)$_2$(P^{i}Pr$_2$N^{i}Pr)FeCl] (**9**) is synthesized under the identical reaction conditions of **8**, using $FeCl_2$ in place of $MnCl_2$. The ^{1}H NMR spectrum of **9** exhibits nine broad paramagnetic resonances that span the range of +85 to −39 ppm, attributed to two inequivalent phosphinoamide environments. It was later determined crystallographically that this inequivalence is due to one of the phosphinoamide ligands coordinating in the opposite direction from the other two in complexes **8** and **9** (vide infra).

Molecular Structures of 3−9. As predicted, X-ray crystallographic studies reveal that complexes **3** and **4** are isomorphous and adopt unusual structures in which the bimetallic core consists of three symmetric six-membered $M_2N_2P_2$ rings (Figure 1, Supporting Information). The coordination environment about the amide-bound Mn2 center in **3** is trigonal planar (Σ_{N-Mn-N} 356.99°) and the distorted tetrahedral coordination sphere of Mn1 is completed by a terminal phosphinoamide ligand. It is clear from the molecular structure that the Mn^{II} ions adopt different coordination

dx.doi.org/10.1021/ic300776y | Inorg. Chem. 2012, 51, 8225−8240

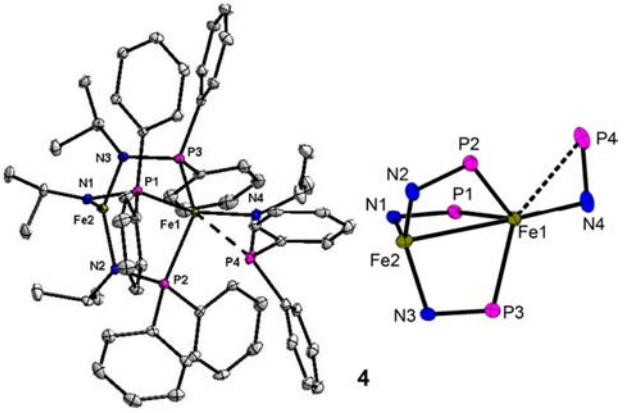

Figure 1. Displacement ellipsoid (30%) representations of **4** (complex **3** is isomorphous, see Supporting Information). Hydrogen atoms have been omitted for clarity. Selected bond lengths (Å) and angles (deg): **4**: Fe1−Fe2, 2.8684(6); Fe1−P1, 2.4593(8); Fe1−P2, 2.4791(8); Fe1−P3, 2.5355(8), Fe1−P4, 2.8129(9); Fe1−N4, 1.944(2); Fe2−N1, 1.946(2); Fe2−N2, 1.953(2); Fe2−N3, 1.960(2); N1−Fe2−N2, 121.16(9); N1−Fe2−N3, 118.17(9); N2−Fe2−N3, 118.17(9), Fe1−N4−P4, 102.05(12). **3**: Mn1−Mn2, 3.1436(3); Mn1−P1, 2.6093(4); Mn1−P2, 2.5843(4); Mn1−P3, 2.6424(4); Mn1−P4, 2.8384(4); Mn1−N4, 1.9967(13); Mn2−N1, 2.0369(13); Mn2−N2, 2.0304(12); Mn2−N3, 2.0376(12); N1−Mn2−N2, 118.74(5); N1−Mn2−N3, 117.11(5); N2−Mn2−N3, 116.25(5); Mn1−N4−P4, 101.26(6).

environments—Mn2 binds three negatively charged amides while Mn1 is bound by three neutral phosphine donors and one terminal amide—resulting in an unusual zwitterionic homobimetallic complex. In addition to the terminal amide ligand bound to Mn1, the solid state structure suggests an additional weaker interaction with the pendant phosphine (Mn1−P4 = 2.8384(4) Å). The terminal Mn1−N distance is 0.04 Å shorter than that of Mn2 with the bridging phosphinoamides, likely a result of additional amide π-donation to the more electronically unsaturated Mn1. The Mn−N distances are comparable to those in the previously reported heterobimetallic Mn/Cu complex supported by this ligand system, $Mn(^{i}PrNPPh_2)_3Cu(Ph_2PNH^{i}Pr)$,[51] and the average Mn−P distance in **3** (2.6120(4) Å) is comparable to that in the few examples of tris(phosphine)-supported pseudotetrahedral Mn^{II} complexes.[55] The interatomic distance between the Mn ions in **3** is significantly longer than the sum of the covalent radii (3.1436(3) Å vs 2.354 Å),[56,57] suggesting little or no bonding interaction between the metal ions.

An X-ray crystallographic study shows that single crystals of **4** are isomorphous with those of **3**; however, there are subtle differences in their geometrical parameters (Figure 1). Most notably, the Fe−N and Fe−P distances in **4** are substantially shorter than the Mn−N and Mn−P distances in complex **3**. This phenomenon can be attributed to the higher spin, *S*, of the Mn^{II} centers resulting in poor ligand field stabilization. Interestingly, only two tris(phosphine) iron amide complexes have been reported in the literature, the zwitterionic Fe^{II} tris(phosphino)borates $PhB(CH_2PPh_2)_3Fe(NHtolyl)$ and $PhB(CH_2P^{i}Pr_2)_3FeNPh_2$.[58,59] The Fe1−P distances and Fe1−N4 distances in **4** (avg Fe−P = 2.49 Å; Fe1−N4 = 1.944(2) Å) are consistent with these two complexes (e.g., avg Fe−P = 2.42 Å and Fe−N = 1.913(2) Å in $PhB(CH_2P^{i}Pr_2)_3FeNPh_2$).[58] In addition, the Fe2−N distances in **4** (avg = 1.95 Å) are similar to those in the previously reported Fe^{II} complex $Fe(^{i}PrNPPh_2)_3Cu(Ph_2PNH^{i}Pr)$ (avg = 1.97 Å).[51] Thus, bond metrics are consistent with both Fe centers remaining in a 2^+ oxidation state. As with **3**, the interatomic distance between the Fe centers in **4** is significantly longer than the sum of the covalent radii (2.8684(6) Å vs 2.346 Å),[56,57] indicative of weak or absent metal−metal bonding interactions.

A single crystal X-ray structure determination of **5** reveals two bridging phosphinoamide ligands, a μ_2-Cl, and terminally bound phosphinoamide and THF ligands on either Mn center (Figure 2). The geometry at both four-coordinate Mn centers is nearly tetrahedral (avg angles: 109.5° and 108.4°, respectively), with the largest deviation being the N1−Mn1−N2 angle (129.68(6)°), which is expanded as a result of the steric bulk of the mesityl amide substituents. In contrast to **3**, the amide-bound Mn center in **5** has only two amide-donors, resulting in a more electronically unsaturated metal and necessitating binding of an additional THF solvent molecule. As seen in **3** and **4** the pendant phosphine donor bound to the terminal amide ligand is only weakly interacting with Mn2 (Mn2−P3 = 3.0933(6) Å).

The solid state molecular structure of **6** reveals a C_3 symmetric dimer consisting of three symmetrical bridging phosphinoamides and a chloride at the terminal position on the phosphine-bound Fe center (Figure 2). Similar to **4**, the geometries at the two Fe centers are best described as trigonal planar about Fe1 (Σ_{N-Fe-N} 359.89°) and pseudotetrahedral

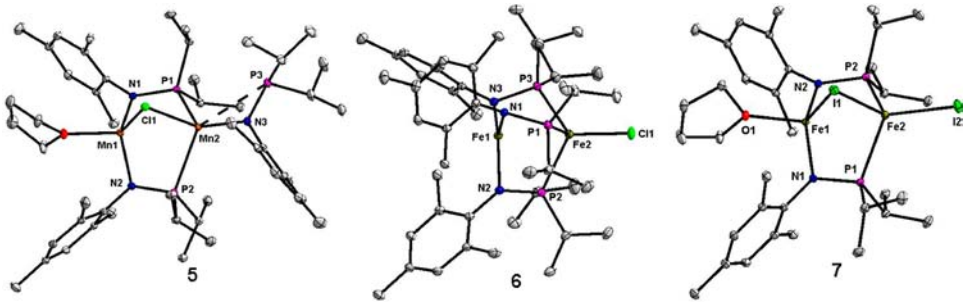

Figure 2. Displacement ellipsoid (30%) representations of **5**, **6**, and **7**. Hydrogen atoms have been omitted for clarity. Selected bond lengths (Å) and angles (deg): **5**: Mn1−Mn2, 3.0033(4); Mn1−N1, 2.0404(14); Mn1−N2, 2.0397(15); Mn1−O1, 2.1184(13); Mn1−Cl1, 2.4462(5); Mn2−Cl1, 2.5242(5); Mn2−P1, 2.6110(5); Mn2−P2, 2.6205(5); Mn2−P3, 3.0933(6); Mn2−N3, 2.0114(15), Mn2−N3−P3, 112.85(8). **6**: Fe1−Fe2, 2.5855(4); Fe1−N1, 2.0201(15); Fe1−N2, 1.9999(15); Fe1−N3, 1.9959(16), Fe2−P1, 2.4497(6); Fe2−P2, 2.4383(6); Fe2−P3, 2.4546(6); Fe2−Cl1, 2.2630(5); N1−Fe1−N2, 121.56(6); N1−Fe1−N3, 118.25(6); N2−Fe1−N3, 120.08(7). **7**: Fe1−Fe2, 2.8134(3); Fe1−N1, 1.9808(12); Fe1−N2, 1.9542(12); Fe1−O1, 2.0796(11); Fe1−I1, 2.8128(3); Fe2−P1, 2.4702(5); Fe2−P2, 2.4523(4); Fe2−I1, 2.7004(3); Fe2−I2, 2.5729(3); N1−Fe1−N2, 134.89(5); N1−Fe1−O1, 103.44(5); N1−Fe1−I1, 104.19(4); N2−Fe1−O1, 100.15(5); N2−Fe1−I1, 105.25(4); O1−Fe1−I1, 106.31(3).

dx.doi.org/10.1021/ic300776y | *Inorg. Chem.* 2012, 51, 8225−8240

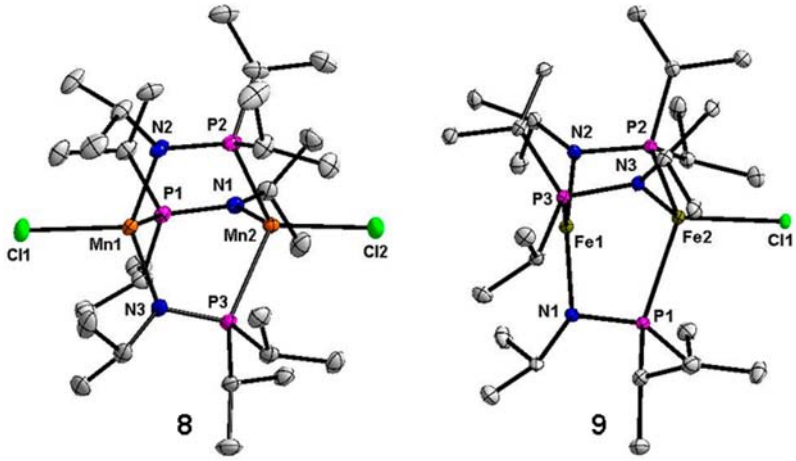

Figure 3. Displacement ellipsoid (30%) representations of **8** and **9**. For clarity, the $[(THF)_3Li]^+$ cation of **8**, one of the two independent molecules in the asymmetric unit of **9**, and all hydrogen atoms have been omitted. Selected bond lengths (Å): For **8**: Mn1−Mn2, 3.2464(9); Mn1−N2, 2.079(3); Mn1−N3, 2.071(2); Mn1−P1, 2.624(1); Mn1−Cl1, 2.439(1); Mn2−P2, 2.574(1); Mn2−P3, 2.582(1); Mn2−N1, 2.053(2); Mn2−Cl2, 2.347(1). For **9**: Fe1−Fe2, 2.6112(7); Fe1−N1, 1.938(3); Fe1−N2, 1.944(3); Fe1−P3, 2.444(1); Fe2−P1, 2.486(1); Fe2−P2, 2.498(1); Fe2−N3, 1.967(3); Fe2−Cl1, 2.3096(9).

Table 1. Mössbauer Parameters for Complexes 4, 6, 7, and 9[a]

	Fe_N		Fe_P	
complex	δ (mm/s)	$\lvert\Delta E_Q\rvert$ (mm/s)	δ (mm/s)	$\lvert\Delta E_Q\rvert$ (mm/s)
4	0.57	2.17	0.51	1.67
6	0.69	2.63	0.63	1.16
7	0.64	2.77	0.83	1.27
9	0.60	1.80	0.60	1.80
$[Fe(^iPrNPPh_2)_3Cu_2(^iPrNPPh_2)]$[51]	0.65	2.05		
$PhB(CH_2P^iPr_2)_3FeCl$[72]			0.58	1.65
$PhB(CH_2P^iPr_2)_3FeNR_2$[72]			0.55	1.75

[a]The parameters for similar monometallic complexes are also provided for comparison.

about Fe2 (avg. bond angle = 109.3°). Like **3** and **4**, the ligand orientation in complex **6** renders the complex zwitterionic. Unlike the aforementioned complexes, however, the intermetallic distance in complex **6** (2.5855(4) Å) is short enough to indicate a metal−metal interaction. This can be rationalized by the fact that the Cl^- is donating far less electron density than the apical phosphinoamide in **4**. The Fe−Fe distance in the symmetrically bridged tetragonal lantern complex $Fe_2(DPhF)_4$ (2.462(2) Å[44,45]) is significantly shorter than those in **4** or **6**. This phenomenon can be tentatively attributed to the two disparate coordination environments of the two Fe centers in **4** and **6** and the resulting differences in orbital energies, leading to poorer overlap between the metal d orbitals. The immediate coordination sphere of Fe2 in complex **6** bears resemblance to the tris(phosphino)borate $Fe^{II}Cl$ systems reported by Peters and co-workers,[60,61] however, the P−Fe2−P angles in **4** and **6** are ∼101−105° while the tris(phosphine)borate complexes have contracted P−Fe−P angles between 90° and 95°.

An X-ray structure determination of the iodide derivative **7** reveals a geometry consisting of two bridging phosphinoamides and a bridging iodide, with a terminal iodide on Fe2 and a bound THF molecule on Fe1 completing the coordination spheres at each end of the bimetallic framework (Figure 2). The bridging iodide is asymmetrically located between the two Fe atoms (Fe1−I1 = 2.8128(3) Å, and Fe2−I1 = 2.7004(3) Å), likely a consequence of the different electronic environments at the two Fe centers. Unlike complex **6**, the Fe−Fe distance in **7** (2.8134(3) Å) precludes any significant metal−metal interaction.

A single crystal X-ray diffraction study of the $[N^iPrP^iPr_2]^-$-ligated Mn complex **8** reveals an asymmetric triply bridged scaffold. Unlike the aforementioned complexes **3**−**7**, the three-bridging phosphinoamide ligands in **8** orient in two different directions, with two amides bound to Mn1 and the third amide bonded to Mn2 (Figure 3). Mn2 completes its coordination sphere with a terminal chloride ligand, while a $LiCl(THF)_3$ unit bonds to Mn1 (see Supporting Information). While the zwitterionic complex **3** maintains a trigonal planar geometry at the tris(amide)-bound Mn center, the bis(amide) bound Mn center in **8** is more electron-deficient and binds tightly to a LiCl salt. Notably, repeated attempts to remove this LiCl salt via extraction into nonpolar solvents were unsuccessful. Similar to **3** and **5**, there is no indication of a Mn−Mn interaction, as the Mn centers in **8** are separated by 3.2464(9) Å.

The solid state molecular structure of complex **9** contains two crystallographically independent molecules with similar geometrical parameters in the unit cell (Figure 3, Supporting Information). The composition of complex **9** is identical to that of **8**, except for the absence of a coordinated LiCl salt. The geometry at Fe1 is distorted trigonal planar ($\Sigma_{L\text{-}Fe\text{-}L}$ 359.26°), with the angle between the amide donors larger than either P−Fe−N angle (N1−Fe1−N2 = 137.17(12)°). At first glance, this distortion seems unusual since the amide donors should be less sterically encumbered than the phosphines. However, examining the opposite side of the molecule, one can see that this

dx.doi.org/10.1021/ic300776y | Inorg. Chem. 2012, 51, 8225−8240

expansion of the N1−Fe-1−N2 angle is due to steric repulsion between the diisopropylphosphine substituents bound to Fe2. Interestingly, a short intermetallic distance (2.6112(7) Å) is observed in **9**, suggesting a metal−metal interaction.

Four coordinate Mn/Fe centers with two phosphines, one amide, and one chloride in monometallic complexes are relatively rare. A tripodal amido-bis(phosphine) Fe complex was reported by Peters and co-workers in 2006,[62] and a similar Mn complex was reported by Arnold et al. in 2008.[63] The bond distances about Fe2 in **9** are similar to those in the amido-bis(phosphine) system,[62] and in Mn complex **8**, which lacks a metal−metal bond, both the bond distances and bond angles associated with Mn2 are similar to those in the tripodal amido-bis(phosphine) complex [^{t}BuNSiMe$_2$N(CH$_2$CH$_2$P^{i}Pr$_2$)$_2$]-MnCl.[63] Pincer type complexes with similar amide bis-(phosphine) coordination environments have also been reported.[64−66]

Mössbauer Spectroscopy. To further examine the electronic structure and coordination environment of diiron complexes **4**, **6**, **7**, and **9**, these complexes were investigated by zero-field ^{57}Fe Mössbauer spectroscopy, and isomer shift and quadrupole splitting data is presented in Table 1. The Mössbauer spectrum of **4** reveals a broad quadrupole doublet that is best modeled by two overlapping signals of equal intensity (Figure 4), as expected for an asymmetric diiron

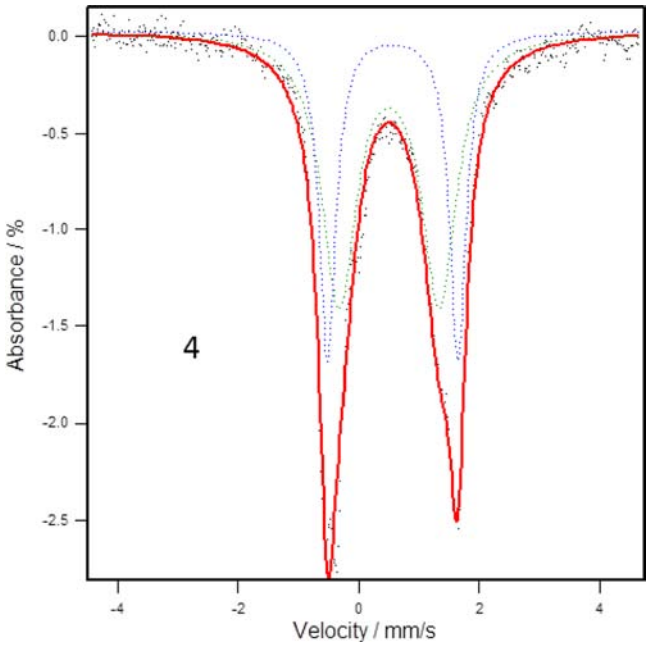

Figure 4. Zero-field ^{57}Fe Mössbauer spectrum of a solid sample of **4** at 110 K (black) fitted as a combination of quadrupole doublets (red) at 55% (δ = 0.57 mm/s, $|\Delta E_Q|$ = 2.17 mm/s, blue) and 45%(δ = 0.51 mm/s, $|\Delta E_Q|$ = 1.67 mm/s, green) intensity.

complex. At first glance, the immediate coordination sphere of each Fe center in complex **4** might suggest a mixed valent Fe^{III}/Fe^{I} configuration; however, the isomer shifts revealed by fitting of the Mössbauer spectrum are consistent with two high spin Fe^{II} centers (δ = 0.57 mm/s, 0.51 mm/s) linked together in a zwitterionic arrangement.[67] Comparing the Mössbauer spectrum of **4** with that of a similar phosphinoamide-linked Fe/Cu$_2$ trimetallic complex, [Fe(^{i}PrNPPh$_2$)$_3$Cu$_2$(^{i}PrNPPh$_2$)] (δ = 0.65 mm/s, $|\Delta E_Q|$ = 2.05 mm/s),[51] the quadrupole doublet centered at δ = 0.57 mm/s ($|\Delta E_Q|$ = 2.17 mm/s) can be assigned as the trigonal planar tris(amido) Fe center in **4** on the basis of similar quadrupole splittings. Other three-coordinate high spin Fe(II) complexes reported in the literature have similar isomer shifts (∼0.6 mm/s to ∼0.8 mm/s).[68−71] The second quadrupole doublet centered at δ = 0.51 mm/s ($|\Delta E_Q|$ = 1.67 mm/s) can, therefore, be attributed to the tetrahedral tris(phosphine)-supported amido-Fe^{II} center. The parameters associated with this Fe center are similar to those reported for Peters' tris(phosphine)borate Fe^{II}-X complexes (X = Cl, δ = 0.58 mm/s, $|\Delta E_Q|$ = 1.65 mm/s; X = NR$_2$, δ = 0.55 mm/s, $|\Delta E_Q|$ = 1.75 mm/s), particularly given the inherent differences (weak interactions between the pendant phosphine and other Fe center) between the former complexes and complex **4**.[72]

Zero-field ^{57}Fe Mössbauer spectra of the [^{i}Pr$_2$PNMes]$^{-}$-substituted complexes **6** and **7** are also composed of two distinct quadrupole doublets, consistent with two Fe centers in disparate coordination environments (Figure 5). The Mössbauer spectrum of complex **6** is adequately fitted by two quadrupole doublets centered at δ = 0.63 $^{mm}/_{s}$ ($|\Delta E_Q|$ = 1.16 mm/s) and δ = 0.69 mm/s ($|\Delta E_Q|$ = 2.63 $^{mm}/_{s}$), indicative of high spin Fe^{II}.[67] While the intensity ratio should be 1:1 based on the stoichiometry of the complex, the best fit was obtained with a 38% contribution of the former signal and a 62% contribution of the latter doublet. We attribute these deviations from 50% to a minor impurity in the sample, likely due to oxidation during sample preparation.[73] Again, based on comparisons to the aforementioned trigonal planar tris(amido) Fe/Cu$_2$ trimetallic and tris(phosphino)borate Fe^{II}-X complexes,[51,72] the doublet with larger quadrupole splitting centered at δ = 0.69 is attributed to the tris(amido) Fe center while the doublet at δ = 0.63 $^{mm}/_{s}$ with smaller quadrupole splitting is assigned as the tris(phosphine)-ligated Fe center.

In contrast to the above compounds, zero-field ^{57}Fe Mössbauer spectroscopy of **9** reveals a single quadrupole doublet centered at δ = 0.60 mm/s ($|\Delta E_Q|$ = 1.80 mm/s, Figure 6). The quadrupole splitting is, again, consistent with high spin Fe^{II}, but the two Fe centers are electronically similar enough to preclude distinction of the two Fe centers by Mössbauer spectroscopy. Coincidental overlap of the Mössbauer signals for the two Fe centers in **9** is consistent with the more similar coordination environment of the two Fe centers in comparison to **6** or **4**.

Magnetism. To better examine the effects of metal−metal interactions in complexes **3**−**9** on their magnetic properties, magnetic susceptibility measurements were carried out in both solution (via Evans' method) and the solid state (via a superconconducting quantum interference device, SQUID). In general, the magnetic behavior of the diiron and dimanganese complexes is different and will be discussed separately.

The solution magnetic moment of **4** at room temperature (μ_{eff} = 9.26 μ_B) is consistent with two high spin S = 2 Fe centers ($\mu_{spin\ only}$ = 9.80 μ_B). To probe the magnetic behavior of **4** at low temperature, the solid state magnetic susceptibility was measured using SQUID magnetometry. A plot of χT as a function of temperature (per mole of Fe in **4**) is shown in Figure 7. The value of χT is virtually constant from room temperature down to near 20 K, below which a small decrease (∼20%) is observed. The solid line shows a fit of the data to a dimer model with g = 2.43(1) and a single ion anisotropy (D) of −3.4(3) cm^{-1}, with J = 0 K, and the spin Hamiltonian used to fit the data is shown in eq 1 (where D is D/kT). Although the data could be fit well using only a single-ion anisotropy term, it is likely that it could be fit similarly with a very weak

dx.doi.org/10.1021/ic300776y | Inorg. Chem. 2012, 51, 8225−8240

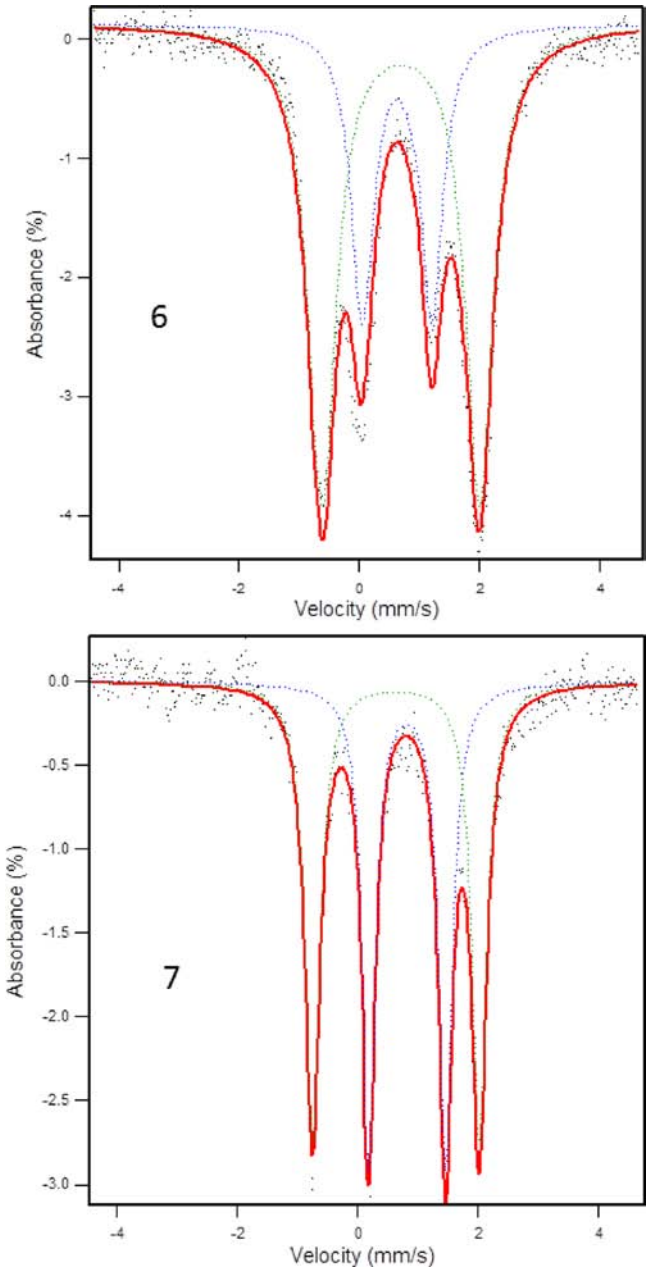

Figure 5. Zero-field ^{57}Fe Mössbauer spectra of solid samples of **6** and **7** at 110 K (black) fitted as a combination of quadrupole doublets (red). For complex **6**, the signal is best fitted with a combination of two signals at 38% (blue; δ = 0.63 mm/s, $|\Delta E_Q|$ = 1.16 mm/s) and 62% (green; δ = 0.69 mm/s, $|\Delta E_Q|$ = 2.63 mm/s) intensity. The deviation of these values from 50% is likely attributed to a minor impurity in the sample. The spectrum of complex **7** is adequately modeled by two signals of roughly equal intensity (blue: 51%, δ = 0.83 mm/s, $|\Delta E_Q|$ = 1.27 mm/s; green, 49%, δ = 0.64 mm/s, $|\Delta E_Q|$ = 2.77 mm/s).

antiferromagnetic exchange. Thus, in the case of **4**, it appears that measurable magnetic superexchange is not present within the complex in either the solid state or solution. Notably, the formamidinate-linked $Fe^{II}Fe^{I}$ and $Fe^{II}Fe^{II}$ systems originally reported by Cotton and co-workers display ferromagnetic behavior, perhaps as a result of significantly shorter metal–metal distances.[40−44]

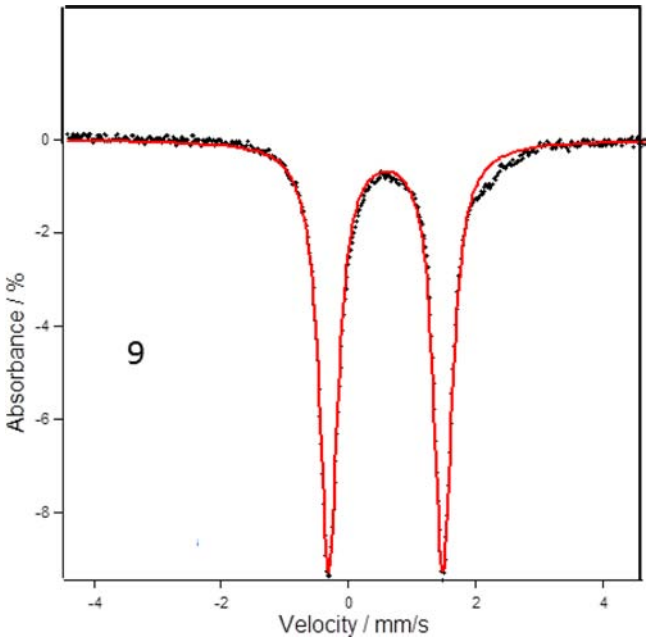

Figure 6. Zero-field ^{57}Fe Mössbauer spectrum of solid samples of **9** at 110 K (black) fitted as a single quadrupole doublet (red, δ = 0.60 mm/s, $|\Delta E_Q|$ = 1.80 mm/s).

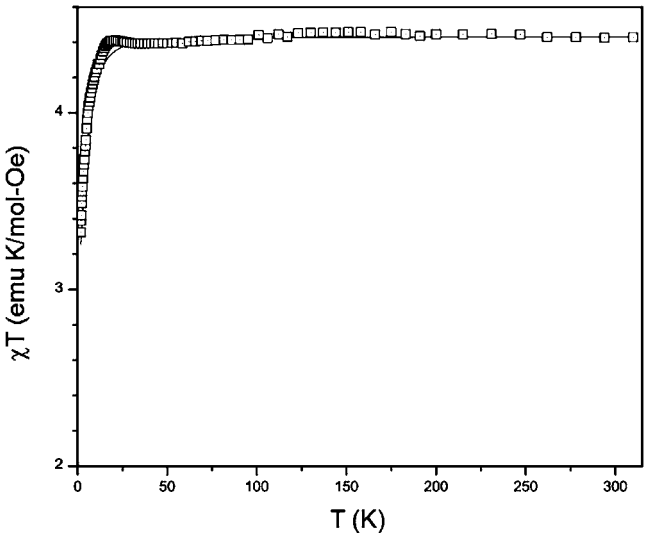

Figure 7. Variable temperature magnetic susceptibility of **4**, reported per mole Fe (rather than per mole complex). Solid line represents a fit to the data as described in the text.

$$\chi = 0.375(g^2)\left(\left(\frac{(6e^{D} + 4e^{-2D})}{e^{2D} + 2e^{D} + 2e^{-2D}}\right) + \frac{2\frac{2(9e^{D} - 7e^{D} - 2e^{-2D})}{D}}{e^{2D} + 2e^{D} + 2e^{-2D}}\right)/9(T - \theta) \quad (1)$$

In contrast, the dimanganese complexes display magnetic behavior indicative of significant antiferromagnetic exchange within the complexes. Complex **3** has a magnetic moment at room temperature in solution (μ_{eff} = 10.33 μ_B) that is slightly below the spin-only value of 11.83 μ_B expected for two S = 5/2 ions. Solid state SQUID measurements suggest antiferromag-

dx.doi.org/10.1021/ic300776y | Inorg. Chem. 2012, 51, 8225−8240

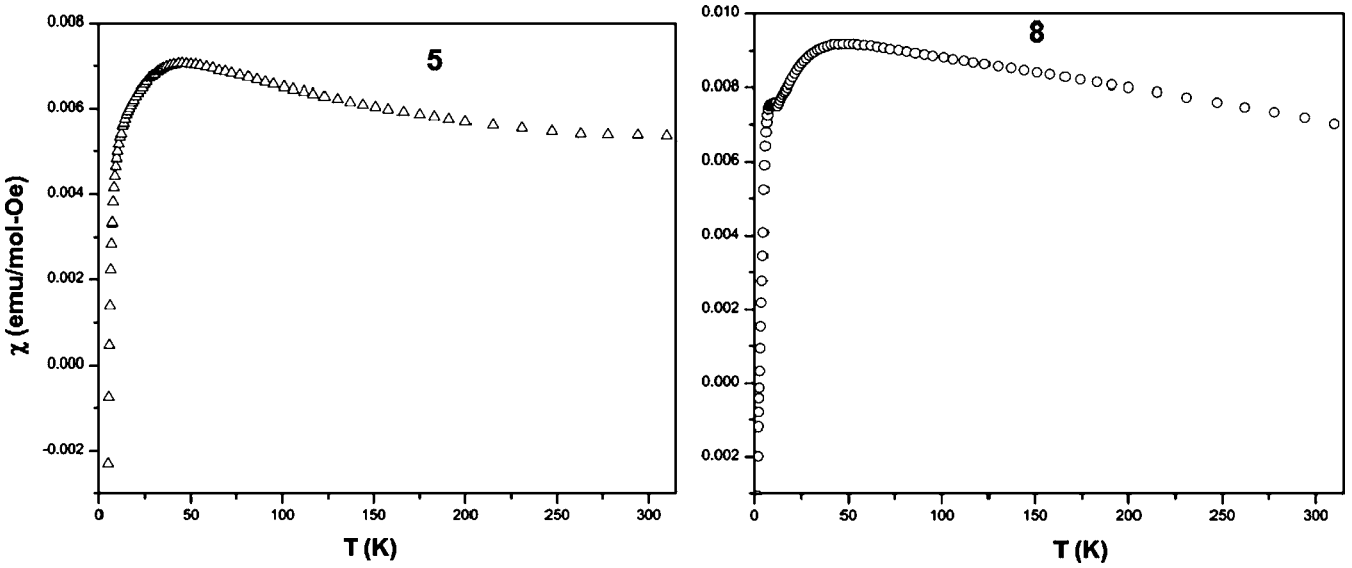

Figure 8. Variable temperature magnetic susceptibility of **5** and **8**, with contributions for a small (4−8%) paramagnetic impurity subtracted out. χ is reported per mole of Mn.

netic coupling between the two Mn(II) centers. However, the magnetic behavior of **3** is dominated by the presence of a paramagnetic impurity to the extent that no meaningful interpretation is presented here (see Supporting Information).[74] The Mn(II) centers in complexes **5** and **8** are also antiferromagetically coupled, this time with a solution magnetic moment significantly lower than the expected spin-only value for two $S = 5/2$ ions (6.91 μ_B and 6.87 μ_B, respectively).[75] Further analysis of these results are presented below.

Magnetization data as a function of field was collected on the halide-bridged complex **5** from 0 kOe to 50 kOe at 1.8 K. Several data points were also collected as the field was reduced to zero to check for hysteresis effects; none were observed (see Supporting Information). Even at 5 kOe, the magnetization of the sample has clearly not reached an appreciable percentage of the saturation magnetization. For a dimanganese complex, such as **5**, the saturation magnetization should approach 60,000 emu/mol, but even at 5 kOe the moment has yet to reach 2000 emu/mol (see Supporting Information). This suggests that either there are significant antiferromagnetic interactions in the sample, or that the bulk of the sample is in a singlet ground state at low temperature and the moment observed at 1.8 K is due to the presence of a small amount of a paramagnetic impurity.[74] The latter interpretation is borne out by the susceptibility data. Magnetic susceptibility data were collected as a function of temperature in a 1 kOe applied field from 1.8 to 310 K. An initial plot of χ vs T reveals that the susceptibility rises continuously as temperature decreases to a maximum near 0.10 emu/mol-Oe at 1.8 K, suggestive of a paramagnetic system (see Supporting Information). However, if this were strictly a paramagnetic dimanganese complex with no interactions, the value of χ at 1.8 K should be 4.89 emu/mol-Oe, nearly 50 times the observed value. Again, this is suggestive of an antiferromagnetic material, but one where the observed susceptibility is dominated by a paramagnetic impurity. Estimating the percentage impurity to be ∼4% from the M vs H plot, the contribution of the paramagnetic impurity was subtracted from the susceptibility data, and the result is shown in Figure 8, with χ reported per mole of Mn rather than per mole of **5**. The data show a maximum in χ near 45 K and then a rapid decrease at lower temperatures as expected for an antiferromagnetic bimetallic species. Attempts to fit the data to an $S = 5/2$ (per Mn) bimetallic model were unsuccessful (likely due to the error introduced by removal of the paramagnetic impurity contribution which accounted for ∼50% of the observed susceptibility at 40 K), but do suggest a J value in the range −5 to −8 K.

The antiferromagnetic behavior of complex **5** is, perhaps, expected given the presence of a halide bridging the two Mn centers. However, similar magnetic susceptibility results were observed for complex **8**, which lacks a bridging halide. The M vs H data at 1.8 K is similarly lower than anticipated for an uncoupled high spin Mn(II) bimetallic system, but shows a slightly larger percentage paramagnetic impurity (the saturation magnetization is approaching 5000 emu/mol at 5 kOe, suggesting an 8% impurity, see Supporting Information).[74] The magnetic susceptibility data again shows only a monotonic increase with decreasing temperature (see Supporting Information). However, subtraction of an 8% paramagnetic impurity results in a maximum near 40 K, similar to that observed for **5**, again indicative of antiferromagnetic interactions in the bulk material (Figure 8).[74] The lack of the chloride bridge in **8**, relative to **5**, suggests that the magnetic superexchange is propagated through the phosphinoamide M-P-N-M bridge.

It is particularly interesting that this phosphinoamide-mediated magnetic superexchange pathway is operative in the Mn(II) bimetallic complexes, but completely absent in the case of the Fe(II) analogues. Since the metal−metal distances in the diiron complexes are significantly shorter than those in the dimanganese complexes (vide supra), it can be concluded that the observed antiferromagnetic coupling in the Mn_2 complexes must occur through the bridging phosphinoamide ligands. The question as to why the phosphinoamide-mediated magnetic superexchange mechanism is operative only in the case of manganese is intriguing, and may relate to better angular overlap between the metal and ligand orbitals once metal−metal bonding interactions are disrupted.

Cyclic Voltammetry. The redox properties of the triply bridged complexes **3**, **4**, **6**, and **8**−**9** were investigated using

dx.doi.org/10.1021/ic300776y | Inorg. Chem. 2012, 51, 8225−8240

cyclic voltammetry (CV). In general, the diiron complexes were found to undergo both oxidative and reductive events, while the dimanganese complexes only displayed oxidative behavior within the measurable THF solvent window. Measured redox potentials are tabulated in Table 2. The CV of dimanganese complex **3** displayed two oxidative events,[76] including a reversible oxidation at $E_{1/2}$ = −0.58 V and an irreversible oxidation at E_{pa} = 0.05 V (Figure 9). In this fully high spin system, these oxidations must correspond to removal of electrons from metal−metal and metal−ligand antibonding orbitals.

Table 2. Redox Potentials of 3, 4, 8, and 9 (vs Fc/Fc^+) Measured by Cyclic Voltammetry[a]

	redox potential			
complex	$M_N^{III/II}$	$M_P^{III/II}$	$M_P^{II/I}$	$M_N^{II/I}$
3	−0.58 V[b]	0.05 V[c]		
4	−0.74 V[c]	−0.24 V[c]	−1.98 V[b]	−2.64 V[d]
8	−0.44 V[c]	−0.23 V[c]		
9	−1.02 V[c]		−2.15 V[d]	−3.03 V[d]

[a]0.4 M [^{n}Bu$_3$N][PF_6] in THF; scan rate 100 mV/s. [b]$E_{1/2}$ for a reversible process. [c]E_{pa} for an irreversible oxidation. [d]E_{pc} for an irreversible reduction.

In contrast, the CV of the analogous diiron complex **4** displays much richer redox properties with two quasi-reversible oxidative events at E_{pa} = −0.74 V and E_{pa} = −0.24 V, as well as two reductive events (the additional oxidative feature that appears at slightly more negative potential was shown to be an artifact that is not present in the absence of scans to negative potentials, see Supporting Information). The first reduction appears at $E_{1/2}$ = −1.98 V and is fully reversible, while the second reductive feature is an irreversible reduction at E_{pc} = −2.64 V (Figure 9). In this case, reduction involves the addition of electrons to metal−metal bonding orbitals with little metal−ligand antibonding character. The CV of MesNP^{i}Pr$_2$-linked diiron complex **6** also displays both oxidative and reductive features, although in this case interpretation of the CV is not as straightforward on account of very broad features (see Supporting Information). Comparing the oxidation potential of the Fe/Cu complex Fe(^{i}PrNPPh$_2$)$_3$Cu(Ph$_2$PNH^{i}Pr) we recently reported (E_{pa} = −0.60 V)[51] to those of **4**, it can be concluded that more facile first oxidation of **4** involves the tris(amide)-ligated iron center, while the second oxidation occurs at the tris(phosphine)-ligated Fe center. Since no reductive features were observed in the CV of the Fe/Cu complex Fe(^{i}PrNPPh$_2$)$_3$Cu(Ph$_2$PNH^{i}Pr), it can also be concluded that the reduction of **4** at −1.98 V is centered on the tris(phosphine)ligated Fe center.[51] This is also consistent with the facile reduction chemistry of other tris(phosphine)Fe complexes in the literature.[61,77] While assigning redox events to each metal individually appears reasonable in this case, it should be noted that this explanation is an oversimplification since a significant amount of d-orbital mixing occurs between the two metals (vide infra).

Similar to dimanganese complex **3**, the CV of complex **8** has oxidative features, although in this case they are both irreversible (see Supporting Information). The shift in potentials of these two oxidations (E_{pa} = −0.44 V and −0.23 V) with respect to **3**—one to more positive potential and one to more negative potential—reflect the asymmetric coordination environments of the two Mn centers in this complex. Diiron complex **9**, again, displays more complex redox behavior in its cyclic voltammogram, with a reversible oxidation at −1.01 V and several irreversible reductive features at E_{pc} = −2.15 V and −3.03 V (Figure 9). The negative shift in oxidation potential with respect to **4** can be attributed to the more electron-donating ^{i}Pr substituents on the phosphine donors, also leading to more negative reduction potentials.

Theoretical Investigations. To gain further insight into the metal−metal interactions in these homobimetallic complexes, and to assess the effects of inequivalent coordination spheres on the orbital interactions between two otherwise identical metal centers, a computational investigation was undertaken using density functional theory (DFT, Gaussian

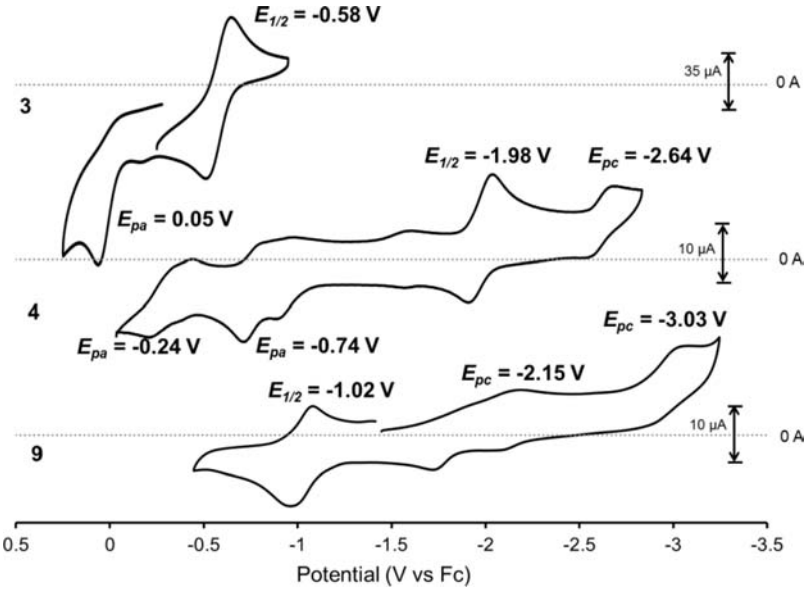

Figure 9. Cyclic voltammograms of **3**, **4**, and **9** (~2 mM analyte in 0.4 M [^{n}Bu$_4$N][PF_6] in THF, scan rate: 100 mV/s). Potentials are reported versus the ferrocene/ferrocenium redox couple. Since reductive features were absent in the case of complex **3**, only the oxidative portion of the cyclic voltammogram is shown for clarity (a full CV is reported in the Supporting Information).

dx.doi.org/10.1021/ic300776y | Inorg. Chem. 2012, 51, 8225−8240

09). Starting from crystallographically derived coordinates, the geometries of **4**, **6**, and **9** were optimized to a minimum. The frontier molecular orbital diagram of **4** is complicated by both significant ligand-based contributions and the reduced symmetry resulting from the fourth phosphinoamide ligand bound to the apical position of the tris(phosphine)Fe center (see Supporting Information). However, significant d orbital mixing can be seen in the calculated frontier MO diagram and it is clear from the computational results that the unpaired electrons reside almost equally on both Fe centers (Mulliken spin densities: Fe_N = 3.77; Fe_P = 3.45, Table 3).

Table 3. Calculated Wiberg Bond Indices (WBIs) and Mulliken spin densities on the two Fe centers in compexes 4, 6, and 9

		Mulliken spin density	
complex	WBI	Fe_P	Fe_N
4	0.34	3.45	3.77
6	0.42	3.35	3.71
9[a]	0.43	3.48	3.42

[a]Fe_N here refers to the Fe center with two coordinated amides and one phosphine donor while FeP refers to the Fe center with two coordinated phosphines and one amide.

The calculated frontier molecular orbital diagram of the more symmetric halide-bound complex **6** is more easily interpreted (Figure 10). First, it should be noted that more than 10 largely metal-based molecular orbitals are shown in Figure 10. This is a result of substantial ligand contributions to several of the singly occupied molecular orbitals (SOMOs). For example, there are two SOMOs shown in Figure 10 that appear to be Fe−Fe σ^* in character, the difference between them is that one is π-bonding with respect to the amide-based p orbitals while the other is Fe−N π-antibonding. The lowest energy, doubly occupied orbital shown in Figure 10 is clearly an Fe−Fe σ bond formed via overlap of two d_{z^2} orbitals. While most of the frontier MOs contain contributions from both metal centers, minimal π- and δ-bonding contributions are present as a result of the disparate energies of the d orbitals of the two Fe centers with different ligand donor sets. Moreover, as previously reported for other high spin diiron complexes, since metal−metal bonding and antibonding orbitals are occupied to some extent, the maximum bond order even in a symmetric complex would be 1.[40−45]

While the calculated frontier MO diagram of **9** is less complicated by ligand contributions based on the absence of aryl substituents, the C_3-symmetric ligand framework is disrupted as the two metals now have 2:1 combinations of donor ligands (Figure 11). As a result of the mixed donor environments in **9**, the unpaired spin density resides almost equally on the two Fe centers (Fe_{N2P}: 3.42; Fe_{NP2}: 3.48, Table 3). As in **6**, more than 10 d-orbital-derived MOs are shown in Figure 11 as a result of substantial orbital contributions to the SOMOs. An Fe−Fe σ-bonding orbital is again seen as one of the doubly occupied frontier MOs, and in this case several orbital combinations with the proper symmetry for π-overlap are visible.

To gain more quantitative insight into the metal−metal interactions in **4**, **6**, and **9**, natural bond orbital (NBO) calculations were performed, and the resulting Fe−Fe NBOs are shown in Figure 12. For complexes **4** and **6** only σ-bonding NBOs were found. In both cases, the NBOs had stronger contributions from the tris(amido)Fe center, but this was more

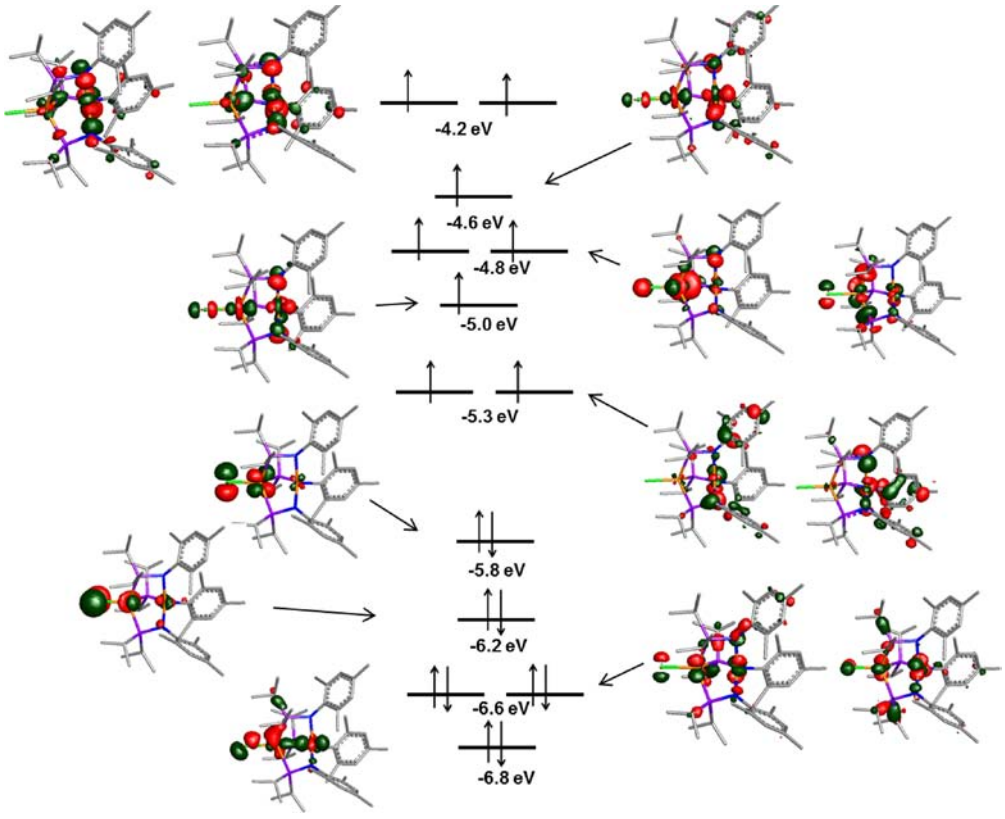

Figure 10. Calculated frontier molecular orbital diagram of complex **6** (BP86/LANL2TZ(f)/6-311+G(d)/D95 V).

dx.doi.org/10.1021/ic300776y | *Inorg. Chem.* 2012, 51, 8225−8240

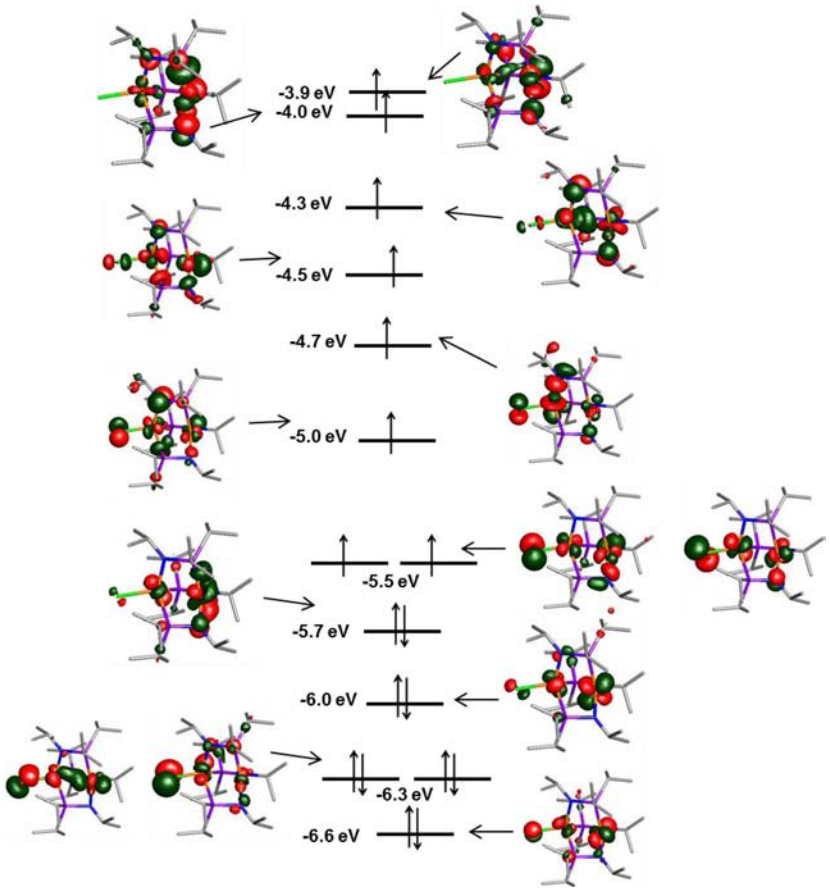

Figure 11. Calculated frontier molecular orbital diagram of complex **9** (BP86/LANL2TZ(f)/6-311+G(d)/D95 V).

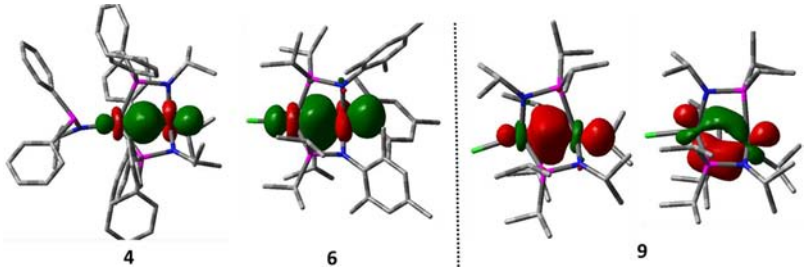

Figure 12. Pictorial representations of the Fe−Fe NBOs of **4**, **6**, and **9**. Composition of Fe−Fe NBO of **4**: 32.3% Fe_P (75.8% d, 16.6% p, 7.6% s); 67.7% Fe_N (91.2% d, 7.9% s). Composition of Fe−Fe NBO of **6**: 45.3% Fe_P (69.6% d, 16.6% p, 13.8% s); 54.7% Fe_N (93.0% d, 5.9% s). Composition of Fe−Fe NBOs of **9**: σ - 50.9% Fe_P (68.1% d, 30.7% s); 49.1% Fe_N (48.2% d, 41.0% p, 10.8% s). π - 52.2% Fe_P (86.1% d, 9.8% p, 4.1% s); 47.8% Fe_N (84.2% d, 14.5% p).

pronounced in the Fe−Fe NBO of complex **4**, likely a result of competing interactions with the additional phosphinoamide ligand. Since one metal center contributes substantially more electron density to the metal−metal bond, this interaction can be seen as dative in nature, with the electron-rich phosphine-ligated Fe center donating electron density to the amide-ligated Fe center. The dative character in this interaction, however, is certainly less pronounced than in a complex composed of two different metal centers, such as an early/late heterobimetallic complex. The tris(amido)Fe contribution to the Fe−Fe σ-bonding NBO in both cases is largely composed of d character, while the tris(phosphine)Fe atom's contribution to bonding contains substantial s and p character as well. The Wiberg bond index (WBI) calculated for the Fe−Fe bond in complex **4** is 0.34 (compared to ∼0.6 for the Fe−P dative bonds), suggestive of a bond order significantly lower than 1 (Table 3). This is consistent with the rather long Fe−Fe distance (2.8684(6) Å) observed in the solid state structure of **4**. For the Fe−Fe bond in **6**, the calculated WBI is slightly higher (0.42), in accordance with the shorter Fe−Fe distance observed for **6** (2.5855(4) Å). The origin of this difference is, again, competing interactions with the apical phosphinoamide donor in **4**.

In the case of complex **9**, both σ- and π-bonding NBOs were found. In both of these orbitals, the contributions from each Fe center to the metal−metal bonding NBOs were essentially equivalent as a result of more similar coordination environments in this complex. As expected, the π-bonding NBO is largely composed of d orbital character; however, the Fe−Fe σ-bonding NBO has substantial s character (30.7%) from the bis(phosphine)-ligated Fe center and substantial p character

dx.doi.org/10.1021/ic300776y | *Inorg. Chem.* 2012, 51, 8225−8240

Table 4. Crystallographic Data and Refinement Parameters for 3, 4, 5 and 6

	3·0.5 Et_2O	4	5	6·pentane
chemical formula	$C_{62}H_{73}Mn_2N_4O_{0.5}P_4$	$C_{60}H_{68}Fe_2N_4P_4$	$C_{49}H_{83}Cl_1Mn_2N_3O_1P_3$	$C_{50}H_{87}Cl_1Fe_2N_3P_3$
fw	1116.04	1081.81	968.45	970.33
T (K)	120	120	120	120
λ (Å)	0.71073	0.71073	0.71073	0.71073
a (Å)	12.6984(5)	12.6193(9)	8.6509(4)	12.3024(4)
b (Å)	44.4400(13)	44.242(3)	26.9140(11)	14.4580(4)
c (Å)	11.7591(3)	11.7062(7)	21.7536(9)	16.5435(5)
α (deg)	90	90	90	101.105(2)
β (deg)	116.967(1)	117.149(3)	91.192(2)	91.933(2)
γ (deg)	90	90	90	112.297(1)
V (Å^3)	5914.3(3)	5815.6(7)	5063.8(4)	2653.02(14)
space group	$P2_1/c$	$P2_1/c$	$P2_1/c$	$P\bar{1}$
Z	4	4	4	2
D_{calc} (g/cm^3)	1.253	1.234	1.270	1.215
μ (cm^{-1})	5.77	6.49	6.84	7.22
R1 ($I > 2\sigma(I)$), wR2[a](all)	0.0778, 0.0829	0.0476, 0.0959	0.0336, 0.0836	0.0410, 0.1198
R_{int}	0.034	0.082	0.053	0.044
N_{ref}(all), N_{ref}($I > 2\sigma(I)$)	17214, 14249	12677, 8253	12814, 9411	15469, 11542

[a] $R1 = \sum||F_o| - |F_o||/\sum|F_o|$; $wR2 = \{\sum[w(F_o^2 - F_c^2)_2]/\sum[w(F_o^2)^2]\}^{1/2}$.

Table 5. Crystallographic Data and Refinement Parameters for 7, 8 and 9

	7	8	9
chemical formula	$C_{34}H_{58}Fe_2I_2N_2O_1P_2$	$C_{39}H_{88.6}Cl_2LiMn_2N_3O_3P_3$	$C_{27}H_{63}Cl_1Fe_2N_3P_3$
fw	938.30	928.36	669.88
T (K)	120	120	120
λ (Å)	0.71073	0.71073	0.71073
a (Å)	9.3067(6)	11.866(2)	11.3057(4)
b (Å)	10.8588(8)	12.897(3)	17.9804(7)
c (Å)	21.1880(15)	17.631(4)	18.6204(7)
α (deg)	104.534(3)	90.101(10)	101.656(2)
β (deg)	93.880(3)	93.261(11)	91.054(2)
γ (deg)	106.983(3)	107.517(10)	107.739(2)
V (Å^3)	1959.2(2)	2568.4(9)	3517.9(2)
space group	$P\bar{1}$	$P\bar{1}$	$P\bar{1}$
Z	2	2	4, Z' = 2
D_{calc} (g/cm^3)	1.590	1.200	1.265
μ (cm^{-1})	24.25	7.23	10.57
R1 ($I > 2\sigma(I)$), wR2[a](all)	0.0195, 0.0465	0.0550, 0.1444	0.0472, 0.1191
R_{int}	0.027	0.051	0.070
N_{ref}(all), N_{ref}($I > 2\sigma(I)$)	11290, 9938	13083, 9279	13823, 9411

[a] $R1 = \sum||F_o| - |F_o||/\sum|F_o|$; $wR2 = \{\sum[w(F_o^2 - F_c^2)_2]/\sum[w(F_o^2)^2]\}^{1/2}$.

(41.0%) from the bis(amide)-ligated Fe center. Despite both σ and π contributions to bonding, the WBI calculated for **9** is nearly identical to that of **6** (0.43), which is in agreement with their very similar Fe−Fe distances (2.6112(7) Å for **9**).

CONCLUSION

In summary, we have successfully isolated and structurally characterized a series of homobimetallic manganese and iron phosphinoamides complexes. The complexes formed via this one-pot synthetic route varied with the identity of the metal halide precursor and the phosphorus and nitrogen substituents. Structural and magnetic characterization of bimetallic complexes **3**−**9** revealed that the metal centers remain in a high spin M^{II} state in these complexes, and Mössbauer spectroscopy of the diiron derivatives confirms the assignment of high spin Fe(II) for both metal centers. The solid state molecular structures revealed relatively long intermetallic distances in the dimanganese complexes, whereas the C_3-symmetric diiron complexes had Fe−Fe distances indicative of some degree of orbital overlap. Computational studies confirmed the presence of weak metal−metal bonding in these high spin systems. Interestingly, magnetic studies revealed that while there were negligible magnetic interactions between the metal centers in the diiron complexes, all of the dimanganese complexes exhibited antiferromagnetic superexchange. Examination of the redox behavior of **3**−**9** using cyclic voltammetry reveals that all of the bimetallic complexes are prone to undergo two sequential one-electron oxidations at mild potentials, and the diiron complexes **4** and **9** also have readily accessible reductive processes. Future studies will focus on systematic investigations of these redox processes and the further reactivity of complexes **3**−**9**.

dx.doi.org/10.1021/ic300776y | Inorg. Chem. 2012, 51, 8225−8240

EXPERIMENTAL SECTION

General Considerations. Unless specified otherwise, all manipulations were performed under an inert atmosphere using standard Schlenk or glovebox techniques. Glassware was oven-dried before use. Benzene, pentane, diethyl ether, tetrahydrofuran, and toluene were dried using a Glass Contours drying column. All solvents were stored over 3 Å molecular sieves. Benzene-d_6 and toluene-d_8 (Cambridge Isotopes) were degassed via repeated freeze−pump−thaw cycles, and dried over 3 Å molecular sieves. THF-d_8 was dried over CaH_2, vacuum-transferred, and degassed via repeated freeze−pump−thaw cycles. Ph_2PNH^iPr,[54,78] $(^iPr)_2PNHMes$,[26] and $(^iPr)_2PNH^iPr$,[26] were synthesized using literature procedures. Anhydrous $MnCl_2$, $FeCl_2$, and FeI_2 were purchased from Strem Chemicals and used after 12 h drying at 100 °C/1 Torr. NMR spectra were recorded at ambient temperature unless otherwise stated on a Varian Inova 400 MHz instrument. Chemical shifts are reported in δ (ppm). For ^1H and ^{13}C NMR spectra the solvent resonance was referenced as an internal standard, and for $^{31}P\{^1H\}$ NMR spectra the 85% H_3PO_4 resonance was referenced as an external standard. IR spectra were recorded on a Varian 640-IR spectrometer controlled by Resolutions Pro software. UV−vis spectra were recorded on a Cary 50 UV−vis spectrophotometer using Cary WinUV software. Elemental analyses were performed at Complete Analysis Laboratory Inc., Parsippany, NJ.

Electrochemistry. Cyclic voltammetry measurements were carried out in a glovebox under a dinitrogen atmosphere in a one-compartment cell using a CH Instruments electrochemical analyzer. A glassy carbon electrode and platinum wire were used as the working and auxiliary electrodes, respectively. The reference electrode was Ag/$AgNO_3$ in THF. Solutions (THF) of electrolyte (0.40 M [$^nBu_4N$][PF_6]) and analyte (2 mM) were also prepared in the glovebox. All potentials are reported versus the ferrocene/ferrocenium couple.

X-ray Structure Determinations. All operations were performed on a Bruker-Nonius Kappa Apex2 diffractometer, using graphite-monochromated MoKα radiation. All diffractometer manipulations, including data collection, integration, scaling, and absorption corrections were carried out using the Bruker Apex2 software.[79] Preliminary cell constants were obtained from three sets of 12 frames. Crystallographic parameters are provided in Tables 4 and 5 and further experimental crystallographic details are described for each compound in the Supporting Information.

Mossbauer Spectroscopy. Iron-57 Mössbauer spectra were measured on a constant acceleration spectrometer (SEE Co, Minneapolis, MN) with a Janis SVT-100 cryostat. Isomer shifts are quoted relative to α-Fe foil (<25 μm thick) at room temperature. The Fe foil standard spectrum has linewidths Γ (fwhm) of 0.292 and 0.326 mm/s for the doublets within the ±4 mm/s window when measured outside the cryostat at room temperature. Samples of **4**, **6**, **7**, and **9** were prepared using approximately 30 mg of sample suspended in paratone-N oil. Data were analyzed using a package written by E. R. King and modified by E. V. Eames in Igor Pro (Wavemetrics) using a simple model consisting of Lorentzian lineshapes with optional asymmetry.

Magnetic Measurements. Solution magnetic moments were measured using Evans' method.[80,81] Crystalline samples of **4**, **5**, and **8** were loaded into gel caps in a dinitrogen-filled glovebox and then sealed with Eicosane wax. The samples were transported in sealed vials under nitrogen, and the waxed capsules were taken directly from the vial, placed in a mounting straw, and the straw loaded into a Quantum Design MPMS measurement system. The sample chamber was immediately evacuated, and filled with He gas. Magnetic susceptibility data were collected as a function of temperature in a 1 kOe applied field from 1.8 to 310 K. Magnetization as a function of field was also collected from 0 kOe to 5 kOe at 1.8 K. Several data points were also collected as the field was reduced to zero to check for hysteresis effects; none were observed (see Supporting Information).

Computational Details. All calculations were performed using Gaussian09-E.01[82] for the Linux operating system. Density functional theory calculations were carried out using a combination of Becke's 1988 gradient-corrected exchange functional[83] and Perdew's 1986 electron correlation functional[84] (BP86). For open shell systems, unrestricted wave functions were used in energy calculations. A mixed-basis set was employed, using the LANL2TZ(f) triple-ζ basis set with effective core potentials for iron,[85−87] Gaussian09's internal 6-311+G(d) for atoms bonded directly to the metal centers (nitrogen and phosphorus), and Gaussian09's internal LANL2DZ basis set (equivalent to D95 V[88]) for carbon and hydrogen. Starting with crystallographically determined geometries as a starting point, when available, the geometries were optimized to a minimum, followed by analytical frequency calculations to confirm that no imaginary frequencies were present. NBO analysis was performed using NBO 3.1,[89] as implemented by Gaussian09. Pictorial representations of molecular orbitals were generated using Jimp 2.[90−92]

[^{i}PrNKPPh$_2$]$_2$ (1). A solution of ^{i}PrNHPPh$_2$ (243 mg, 1.00 mmol) in THF (3 mL) was cooled to −32 °C and added to KH (41 mg, 1.0 mmol) in THF (2 mL). The resulting mixture was stirred at room temperature for 2 h at which point the remaining KH was removed via filtration through Celite. All volatiles were removed in vacuo, and the crude product was washed with pentane (3 × 5 mL) to obtain **1** as an analytically pure pale yellow crystalline solid (250 mg, 89%). ^1H NMR (400 MHz, THF-d_8): δ 7.13 (dd, J_{HP} = 1.2 Hz, J_{HH} = 5.2 Hz, 4H, Ar-*H*), 6.80 (t, J_{HH} = 7.2 Hz, 4H, Ar-*H*), 6.69 (t, J_{HH} = 7.2 Hz, 2H, Ar-*H*), 3.08 (dsept, J_{HP} = 20.8 Hz, J_{HH} = 6.0 Hz, 1H, ^{i}Pr−C*H*), 0.54 (d, J_{HH} = 6.0 Hz, 6H, ^{i}Pr−C*H*$_3$). $^{13}C\{^1H\}$ NMR (100.53 MHz, THF-d_8): δ 154.3 (d, J_{CP} = 40.9 Hz), 132.8 (d, J_{CP} = 10.8 Hz), 127.7 (d, J_{CP} = 3.6 Hz), 125.8 (s), 51.2 (s, ^{i}Pr-CH), 30.8 (d, J_{CP} = 8.5 Hz, ^{i}Pr-CH$_3$). $^{31}P\{^1H\}$ NMR (161.84 MHz, THF-d_8): δ 46.4. Anal. Calcd for $C_{15}H_{17}KNP$: C, 64.03; H, 6.09; N, 4.98. Found: C, 63.91; H, 6.07; N, 4.89.

[MesNKP^{i}Pr$_2$]$_2$ (2). A solution of MesNHP^{i}Pr$_2$ (251 mg, 1.00 mmol) in THF (3 mL) was cooled to −32 °C and added to KH (41 mg, 1.0 mmol) in THF (2 mL). The resulting mixture was stirred at room temperature for 2 h, at which point the remaining KH was removed via filtration through Celite. All volatiles were removed in vacuo, and the crude product was washed with pentane (3 × 5 mL) to obtain **2** as an analytically pure colorless crystalline solid (260 mg, 92%). ^1H NMR (400 MHz, THF-d_8): δ 6.43 (s, 2H, Ar-*H*), 2.25 (s, 6H, Mes-C*H*$_3$), 1.99 (s, 3H, Mes-C*H*$_3$), 1.30 (sept, J_{HH} = 6.8 Hz, 2H, ^{i}Pr−C*H*), 1.04 (overlapped doublets, J_{HH} = 7.6 Hz, J_{HH} = 8.0 Hz, 6H, ^{i}Pr−C*H*$_3$), 0.89 (d, J_{HH} = 7.2 Hz, 3H, ^{i}Pr−C*H*$_3$), 0.86 (d, J_{HH} = 7.2 Hz, 3H, ^{i}Pr−C*H*$_3$). $^{13}C\{^1H\}$ NMR (100.53 MHz, THF-d_8): δ 160.8, 130.5, 129.8, 119.1, 30.7 (d, J_{CP} = 80.2 Hz, ^{i}Pr-CH), 26.5 (s, Mes-C*H*$_3$), 23.1 (d, J_{CP} = 42.3 Hz, ^{i}Pr-CH), 21.0 (s, Mes-C*H*$_3$), 20.5 (d, J_{CP} = 19.8 Hz, ^{i}Pr-CH$_3$), 18.7 (d, J_{CP} = 9.9 Hz, ^{i}Pr-CH$_3$). $^{31}P\{^1H\}$ NMR (161.84 MHz, THF-d_8): δ 72.3. Anal. Calcd for $C_{15}H_{25}KNP$: C, 62.25; H, 8.71; N, 4.84. Found: C, 62.21; H, 8.73; N, 4.79.

[Mn(^{i}PrNPPh$_2$)$_3$Mn(^{i}PrNPPh$_2$)] (3). A solution of $MnCl_2$ (63 mg, 0.50 mmol) in THF (3 mL) was cooled to −32 °C and to this a THF solution (3 mL) of ^{i}PrNKPPh$_2$ (281 mg, 1.00 mmol) was added dropwise over a period of 5−10 min. The reaction mixture was gradually warmed to room temperature and continuously stirred for 12 h. The volatiles were subsequently removed in vacuo, and the remaining crude reddish brown materials were extracted with toluene (3 × 2 mL) and filtered through Celite to remove KCl and other insoluble byproducts. The volatiles were removed from the filtrate under vacuum to obtain analytically pure **3** as a yellow crystalline solid (230 mg, 83%). X-ray quality single crystals were grown by careful layering of pentane onto a concentrated THF solution of **3** at room temperature. UV−vis (THF) λ_{max}, nm (ε, M^{-1} cm^{-1}): 495 (517), 611 (219). Evans' method (THF-d_8): 10.38 μ_B. Anal. Calcd for $C_{60}H_{68}N_4P_4Mn_2$: C, 66.79; H, 6.35; N, 5.19. Found: C, 66.70; H, 6.37; N, 5.21.

[Fe(^{i}PrNPPh$_2$)$_3$Fe(^{i}PrNPPh$_2$)] (4). A solution of $FeCl_2$ (63 mg, 0.50 mmol) in THF (3 mL) was cooled to −32 °C and to this a THF solution (3 mL) of ^{i}PrNKPPh$_2$ (281 mg, 1.00 mmol) was added dropwise over the period of 5 min. The reaction mixture was gradually warmed to room temperature and continuously stirred for 12 h. The volatiles were subsequently removed in vacuo, and the crude purple-brown materials were extracted with Et_2O (3 × 2 mL) and filtered

dx.doi.org/10.1021/ic300776y | Inorg. Chem. 2012, 51, 8225−8240

through Celite. Cooling the concentrated Et_2O solution to −32 °C to afforded analytically pure purple blocks of **4** (160 mg, 59.3%). ^{1}H NMR (400 MHz, C_6D_6): δ 53.7, 31.2, 12.9, 11.5, 10.2, 3.3, 1.1, −3.2, −20.5, −30.9 (bs). UV−vis (C_6H_6) λ_{max}, nm (ε, M^{-1} cm^{-1}): 541 (323). Evans' method (C_6D_6): 9.26 μ_B. Anal. Calcd for $C_{60}H_{68}N_4P_4Fe_2$: C, 66.68; H, 6.34; N, 5.18. Found: C, 66.78; H, 6.25; N, 5.10.

[(THF)Mn(μ-Cl)(MesNP^{i}Pr$_2$)$_3$Mn(MesNP^{i}Pr$_2$)] (5). A solution of $MnCl_2$ (84 mg, 0.67 mmol) in THF (3 mL) was cooled to −32 °C and to this a THF solution (3 mL) of MesNKP^{i}Pr$_2$ (289 mg, 1.00 mmol) was added dropwise over the period of 5 min. The resulting mixture was stirred at room temperature for 12 h, at which time the insoluble materials were removed via filtration through Celite. The volatiles were subsequently removed in vacuo, and the crude product was extracted with toluene and filtered through Celite to remove KCl and other insoluble byproducts. Volatiles were removed from the filtrate under vacuum to obtain analytically pure **5** as a red-orange crystalline solid (230 mg, 71%). X-ray quality single crystals were grown from a THF/pentane mixture of **5** at room temperature. UV−vis (THF) λ_{max}, nm (ε, M^{-1} cm^{-1}): 500 (383), 634 (253), 1059 (400). Evans' method (THF-d_8): 6.91 μ_B. Anal. Calcd for $C_{49}H_{83}ClN_3OP_3Mn_2$: C, 60.77; H, 8.64; N, 4.34. Found: C, 60.73; H, 8.53; N, 4.29.

[Fe(MesNP^{i}Pr$_2$)$_3$FeCl] (6). A solution of $FeCl_2$ (85 mg, 0.67 mmol) in THF (3 mL) was cooled to −32 °C and to this a THF solution (3 mL) of MesNKP^{i}Pr$_2$ (289 mg, 1.00 mmol) was added dropwise over a period of 5 min. The resulting mixture was stirred at room temperature for 12 h, at which point the insoluble materials were removed via filtration. The volatiles were subsequently removed in vacuo, and the crude product was extracted with toluene and filtered through Celite to remove KCl and other insoluble byproducts. Volatiles were removed from the filtrate under vacuum to obtain analytically pure **6** as a pale yellow crystalline solid (170 mg, 57%). ^{1}H NMR (400 MHz, C_6D_6): δ 43.3, 32.6, 29.8, 26.7, 16.6, 3.3. UV−vis (THF) λ_{max}, nm (ε, M^{-1} cm^{-1}): 490 (102), 668 (46). Evans' method (THF-d_8): 6.80 μ_B. Anal. Calcd for $C_{45}H_{75}ClN_3P_3Fe_2$: C, 60.18; H, 8.42; N, 4.68. Found: C, 59.94; H, 8.37; N, 4.53.

[(THF)Fe(μ-I)(MesNP^{i}Pr$_2$)$_2$FeI] (7). A solution of FeI_2 (310 mg, 1.00 mmol) in THF (3 mL) was cooled to −32 °C and to this a cold THF solution (3 mL) of MesNKP^{i}Pr$_2$ (289 mg, 1.00 mmol) was added dropwise over a period of 5 min. The resulting mixture was stirred at room temperature for 12 h, at which point the insoluble materials were removed via filtration through Celite. The volatiles were subsequently removed in vacuo, and the crude product was extracted with toluene and filtered through Celite to remove KI and other insoluble byproducts. The volatiles were removed from the filtrate under vacuum to obtain analytically pure **7** as a brown crystalline solid (340 mg, 74%). ^{1}H NMR (400 MHz, C_6D_6): δ 58.7, 53.7, 40.9, 31.5, 30.8, 30.0, 3.3, 1.3, 1.1, −0.5, −15.3 (bs). UV−vis (C_6H_6) λ_{max}, nm (ε, M^{-1} cm^{-1}): 511 (819). Evans' method (C_6D_6): 8.53 μ_B. Anal. Calcd for $C_{34}H_{58}N_2I_2OP_2Fe_2$: C, 43.52; H, 6.23; N, 2.99. Found: C, 43.48; H, 6.32; N, 3.05.

(THF)$_3$LiCl[Mn(N^{i}PrP^{i}Pr$_2$)$_2$(P^{i}Pr$_2$N^{i}Pr)MnCl] (8). A solution of ^{i}PrNHP^{i}Pr$_2$ (175 mg, 1.00 mmol) in THF (3 mL) was cooled to −32 °C and to this ^{n}BuLi (0.63 mL, 1.6 M in hexanes, 1.0 mmol) was added dropwise over 10 min. The resulting pale yellow solution was warmed to room temperature and stirred for 2 h to form ^{i}PrNLiPPh$_2$ in situ. The resulting mixture was added to a THF solution (3 mL) of $MnCl_2$ (84 mg, 0.67 mmol) at −32 °C, and the reaction mixture was gradually warmed to room temperature and continuously stirred for 12 h. During this time period, the solution became homogeneous and turned red-orange. All volatiles were subsequently removed in vacuo, and the crude materials were dissolved in THF and layered with pentane at room temperature. Red-orange blocks of **8** were obtained after 12 h (176 mg, 56%). UV−vis (THF) λ_{max}, nm (ε, M^{-1} cm^{-1}): 500 (440), 642 (400), 1063 (340). Evans' method (THF-d_8): 6.87 μ_B. Because of both extreme air and moisture sensitivity and the labile solvent molecules on the Li ion, repeated combustion analysis data of **8** was unsatisfactory.

[Fe(N^{i}PrP^{i}Pr$_2$)$_2$(P^{i}Pr$_2$N^{i}Pr)FeCl] (9). A solution of ^{i}PrNHP^{i}Pr$_2$ (175 mg, 1.00 mmol) in THF (3 mL) was cooled to −32 °C and to this ^{n}BuLi (0.63 mL, 1.6 M in hexanes, 1.0 mmol) was added dropwise over 10 min. The resulting pale yellow solution was warmed to room temperature and stirred for 2 h to form ^{i}PrNLiPPh$_2$ in situ. The resulting mixture was added to a THF solution (3 mL) of $FeCl_2$ (85 mg, 0.67 mmol) at −32 °C, and the reaction mixture was gradually warmed to room temperature and continuously stirred for 12 h. During this time period, the solution became homogeneous and brown. All volatiles were subsequently removed in vacuo, and the crude red materials were extracted with ether (3 × 2 mL) and filtered through Celite. The ether solution was again dried in vacuo to obtain analytically pure **9** as a yellow crystalline solid (150 mg, 67.3%).^{1}H NMR (400 MHz, C_6D_6): δ 85.4, 75.2, 64.4, 40.5, 29.9, 4.2, 1.8, −4.7, −38.5 (bs). UV−vis (C_6H_6) λ_{max}, nm (ε, M^{-1} cm^{-1}): 470 (615). Evans' method (C_6D_6): 8.95 μ_B. Anal. Calcd for $C_{27}H_{63}ClN_3P_3Fe_2$: C, 48.41; H, 9.48; N, 6.27. Found: C, 48.33; H, 9.36; N, 6.14.

■ ASSOCIATED CONTENT

Ⓢ Supporting Information

Additional spectral, cyclic voltammetry, magnetic and crystallographic data for complexes **1**−**9** (in CIF format). This material is available free of charge via the Internet at http://pubs.acs.org.

■ AUTHOR INFORMATION

Corresponding Author

*E-mail: thomasc@brandeis.edu.

Notes

The authors declare no competing financial interest.

■ ACKNOWLEDGMENTS

This material is based upon work supported by the Department of Energy under Award No. DE-SC0004019. C.M.T. is grateful for a 2011 Sloan Research Fellowship. The authors also thank Brandeis University for initially funding this project, Prof. Theodore Betley for access to a Mössbauer spectroscopy facility, and Prof. Christopher Landee for insightful discussions related to magnetic data.

■ REFERENCES

(1) Adams, R. D.; Cotton, F. A. *Catalysis by Di- and Polynuclear Metal Cluster Complexes*; Wiley-VCH: New York, NY, 1998.
(2) Tsui, E. Y.; Kanady, J. S.; Day, M. W.; Agapie, T. *Chem. Commun.* **2011**, *47*, 4189−4191.
(3) Zhao, Q.; Harris, T. D.; Betley, T. A. *J. Am. Chem. Soc.* **2011**, *133*, 8293−8306.
(4) Zhao, Q.; Betley, T. A. *Angew. Chem., Int. Ed.* **2011**, *50*, 709−712.
(5) Powers, T. M.; Fout, A. R.; Zheng, S.-L.; Betley, T. A. *J. Am. Chem. Soc.* **2011**, *133*, 3336−3338.
(6) Eames, E. V.; Harris, T. D.; Betley, T. A. *Chem. Sci.* **2012**, *3*, 407−415.
(7) Harris, T. D.; Zhao, Q.; Sanchez, R. H.; Betley, T. A. *Chem. Commun.* **2011**, *47*, 6344−6346.
(8) Kanady, J. S.; Tsui, E. Y.; Day, M. W.; Agapie, T. *Science* **2011**, *333*, 733−736.
(9) Ragsdale, S. W. *J. Inorg. Biochem.* **2007**, *101*, 1657−1666.
(10) Lindahl, P. A.; Graham, D. E. Acetyl-coenzyme A Synthases and Nickel-Containing Carbon Monoxide Dehydrogenases. In *Nickel and Its Surprising Impact in Nature*; John Wiley & Sons, Ltd: Hoboken, NJ, 2007; pp 357−415.
(11) Kim, E.; Chufan, E. E.; Kamaraj, K.; Karlin, K. D. *Chem. Rev.* **2004**, *104*, 1077−1134.
(12) Dismukes, G. C. *Chem. Rev.* **1996**, *96*, 2909−2926.
(13) Friedle, S.; Reisner, E.; Lippard, S. J. *Chem. Soc. Rev.* **2010**, *39*, 2768−2779.

(14) Merkx, M.; Kopp, D. A.; Sazinsky, M. H.; Blazyk, J. L.; Müller, J.; Lippard, S. J. *Angew. Chem., Int. Ed.* **2001**, *40*, 2782−2807.
(15) Tard, C.; Pickett, C. J. *Chem. Rev.* **2009**, *109*, 2245−2274.
(16) Fontecilla-Camps, J. C.; Volbeda, A.; Cavazza, C.; Nicolet, Y. *Chem. Rev.* **2007**, *107*, 4273−4303.
(17) Cotton, F. A.; Murillo, C. A.; Walton, R. A. *Multiple Bonds Between Metal Atoms*; Springer Science and Business Media, Inc.: New York, 2005.
(18) Collman, J. P.; Boulatov, R. *Angew. Chem., Int. Ed.* **2002**, *41*, 3948−3961.
(19) Chisholm, M. H. *Acc. Chem. Res.* **1990**, *23*, 419−425.
(20) Gade, L. H. *Angew. Chem., Int. Ed.* **2000**, *39*, 2658−2678.
(21) Wheatley, N.; Kalck, P. *Chem. Rev.* **1999**, *99*, 3379−3420.
(22) Stephan, D. W. *Coord. Chem. Rev.* **1989**, *95*, 41−107.
(23) Bullock, R. M.; Casey, C. P. *Acc. Chem. Res.* **1987**, *20*, 167−173.
(24) Cooper, B. G.; Napoline, J. W.; Thomas, C. M. *Catal. Rev. - Sci. Eng.* **2012**, *54*, 1−40.
(25) Thomas, C. M. *Comments Inorg. Chem.* **2011**, *32*, 14−38.
(26) Greenwood, B. P.; Forman, S. I.; Rowe, G. T.; Chen, C.-H.; Foxman, B. M.; Thomas, C. M. *Inorg. Chem.* **2009**, *48*, 6251−6260.
(27) Greenwood, B. P.; Rowe, G. T.; Chen, C.-H.; Foxman, B. M.; Thomas, C. M. *J. Am. Chem. Soc.* **2010**, *132*, 44−45.
(28) Krogman, J. P.; Foxman, B. M.; Thomas, C. M. *J. Am. Chem. Soc.* **2011**, *133*, 14582−14585.
(29) Thomas, C. M.; Napoline, J. W.; Rowe, G. T.; Foxman, B. M. *Chem. Commun.* **2010**, *46*, 5790−5792.
(30) Zhou, W.; Napoline, J. W.; Thomas, C. M. *Eur. J. Inorg. Chem.* **2011**, *2011*, 2029−2033.
(31) Simona, M. *Coord. Chem. Rev.* **2009**, *253*, 1793−1832.
(32) Rosenthal, J.; Bachman, J.; Dempsey, J. L.; Esswein, A. J.; Gray, T. G.; Hodgkiss, J. M.; Manke, D. R.; Luckett, T. D.; Pistorio, B. J.; Veige, A. S.; Nocera, D. G. *Coord. Chem. Rev.* **2005**, *249*, 1316−1326.
(33) Gade, L. H. *Angew. Chem., Int. Ed. Engl.* **1996**, *35*, 2089−2090.
(34) Whittlesey, B. R. *Coord. Chem. Rev.* **2000**, *206*−*207*, 395−418.
(35) Xu, Z.; Lin, Z. *Chem.—Eur. J.* **1998**, *4*, 28−32.
(36) Lindahl, P. A. *J. Inorg. Biochem.* **2012**, *106*, 172−178.
(37) Nguyen, T.; Merrill, W. A.; Ni, C.; Lei, H.; Fettinger, J. C.; Ellis, B. D.; Long, G. J.; Brynda, M.; Power, P. P. *Angew. Chem., Int. Ed.* **2008**, *47*, 9115−9117.
(38) Hess, C. R.; Weyhermüller, T.; Bill, E.; Wieghardt, K. *Angew. Chem., Int. Ed.* **2009**, *48*, 3703−3706.
(39) Klose, A.; Solari, E.; Floriani, C.; Chiesi-Villa, A.; Rizzoli, C.; Re, N. *J. Am. Chem. Soc.* **1994**, *116*, 9123−9135.
(40) Cotton, F. A.; Daniels, L. M.; Falvello, L. R.; Matonic, J. H.; Murillo, C. A. *Inorg. Chim. Acta* **1997**, *256*, 269−275.
(41) Cotton, F. A.; Daniels, L. M.; Matonic, J. H.; Murillo, C. A. *Inorg. Chim. Acta* **1997**, *256*, 277−282.
(42) Cotton, F. A.; Feng, X.; Murillo, C. A. *Inorg. Chim. Acta* **1997**, *256*, 303−308.
(43) Zall, C. M.; Zherebetskyy, D.; Dzubak, A. L.; Bill, E.; Gagliardi, L.; Lu, C. C. *Inorg. Chem.* **2012**, *51*, 728−736.
(44) Cotton, F. A.; Daniels, L. M.; Murillo, C. A. *Inorg. Chim. Acta* **1994**, *224*, 5−9.
(45) Timmer, G. H.; Berry, J. F. *C.R. Chim.* **2012**, *15*, 192−201.
(46) Fout, A. R.; Zhao, Q.; Xiao, D. J.; Betley, T. A. *J. Am. Chem. Soc.* **2011**, *133*, 16750−16753.
(47) Lu, D.-Y.; Yu, J.-S. K.; Kuo, T.-S.; Lee, G.-H.; Wang, Y.; Tsai, Y.-C. *Angew. Chem., Int. Ed.* **2011**, *50*, 7611−7615.
(48) Ashley, A. E.; Cooper, R. T.; Wildgoose, G. G.; Green, J. C.; O'Hare, D. *J. Am. Chem. Soc.* **2008**, *130*, 15662−15677.
(49) Chai, J.; Zhu, H.; Stuckl, A. C.; Roesky, H. W.; Magull, J.; Bencini, A.; Caneschi, A.; Gatteschi, D. *J. Am. Chem. Soc.* **2005**, *127*, 9201−9206.
(50) Hatnean, J. A.; Raturi, R.; Lefebvre, J.; Leznoff, D. B.; Lawes, G.; Johnson, S. A. *J. Am. Chem. Soc.* **2006**, *128*, 14992−14999.
(51) Kuppuswamy, S.; Cooper, B. G.; Bezpalko, M. W.; Foxman, B. M.; Powers, T. M.; Thomas, C. M. *Inorg. Chem.* **2012**, *51*, 1866−1873.
(52) Fenske, D.; Maczek, B.; Maczek, K. *Z. Anorg. Allg. Chem.* **1997**, *623*, 1113−1120.
(53) Thapa, I.; Gambarotta, S.; Korobkov, I.; Duchateau, R.; Kulangara, S. V.; Chevalier, R. *Organometallics* **2010**, *29*, 4080−4089.
(54) Poetschke, N.; Nieger, M.; Khan, M. A.; Niecke, E.; Ashby, M. T. *Inorg. Chem.* **1997**, *36*, 4087−4093.
(55) Lu, C. C.; Peters, J. C. *Inorg. Chem.* **2006**, *45*, 8597−8607.
(56) Pauling, L. *The Nature of the Chemical Bond*, 3rd ed.; Cornell University Press: Ithaca, NY, 1960.
(57) For completeness we include the van der Waals radii of Mn (2.05 A) and Fe (2.04 A): Hu., S.-Z.; Zhou, Z.-H.; Robertson, B. E. *Z. Kristallogr.* **2009**, *224*, 375−383.
(58) Brown, S. D.; Peters, J. C. *J. Am. Chem. Soc.* **2004**, *126*, 4538−4539.
(59) Betley, T. A.; Peters, J. C. *J. Am. Chem. Soc.* **2004**, *126*, 6252−6254.
(60) Brown, S. D.; Betley, T. A.; Peters, J. C. *J. Am. Chem. Soc.* **2002**, *125*, 322−323.
(61) Betley, T. A.; Peters, J. C. *Inorg. Chem.* **2003**, *42*, 5074−5084.
(62) Whited, M. T.; Rivard, E.; Peters, J. C. *Chem. Commun.* **2006**, 1613−1615.
(63) Chomitz, W. A.; Mickenberg, S. F.; Arnold, J. *Inorg. Chem.* **2007**, *47*, 373−380.
(64) Adhikari, D.; Basuli, F.; Fan, H.; Huffman, J. C.; Pink, M.; Mindiola, D. J. *Inorg. Chem.* **2008**, *47*, 4439−4441.
(65) Buschhorn, D.; Pink, M.; Fan, H.; Caulton, K. G. *Inorg. Chem.* **2008**, *47*, 5129−5135.
(66) Fryzuk, M. D.; Leznoff, D. B.; Ma, E. S. F.; Rettig, S. J.; Young, V. G. *Organometallics* **1998**, *17*, 2313−2323.
(67) Schunemann, V.; Paulsen, H. Mossbauer Spectroscopy. In *Applications of Physical Methods to Inorganic and Bioinorganic Chemistry*; Scott, R. A., Lukehart, C. M., Eds.; John Wiley & Sons, Ltd.: Hoboken, NJ, 2007; pp 241−269.
(68) Evans, D. J.; Hughes, D. L.; Silver, J. *Inorg. Chem.* **1997**, *36*, 747−748.
(69) Sanakis, Y.; Power, P. P.; Stubna, A.; Munck, E. *Inorg. Chem.* **2002**, *41*, 2690−2696.
(70) MacDonnell, F. M.; Ruhlandt-Senge, K.; Ellison, J. J.; Holm, R. H.; Power, P. P. *Inorg. Chem.* **1995**, *34*, 1815−1822.
(71) Andres, H.; Bominaar, E. L.; Smith, J. M.; Eckert, N. A.; Holland, P. L.; Munck, E. *J. Am. Chem. Soc.* **2002**, *124*, 3012−3025.
(72) Hendrich, M. P.; Gunderson, W.; Behan, R. K.; Green, M. T.; Mehn, M. P.; Betley, T. A.; Lu, C. C.; Peters, J. C. *Proc. Natl. Acad. Sci. U.S.A.* **2006**, *103*, 17107−17112.
(73) Repeated measurements were very similar. Alternative fits that either included this impurity or attempted to fit to doublets of 50% intensity were unsatisfactory. See Supporting Information for more details.
(74) All of the compounds reported herein are highly air sensitive, and were transported and handled outside of an inert atmosphere to collect Mössbauer and SQUID data. Although precautionary measures were taken to prevent exposure to air, it is likely that decomposition occurred to some extent, giving rise to the impurities observed using these techniques.
(75) Repeated measurements gave similar results, indicating that the solution magnetic behavior of these compounds may differ from that in the solid state.
(76) The resting potential was measured to be more negative than −0.6 V, allowing both redox events in the CV of **3** to be assigned as oxidative in nature.
(77) Thoreson, K. A.; Follett, A. D.; McNeill, K. *Inorg. Chem.* **2010**, *49*, 3942−3949.
(78) Sisler, H.; Smith, N. *J. Org. Chem.* **1961**, *26*, 611−613.
(79) *Apex 2: Version 2 User Manual, M86-E01078*; Bruker Analytical X-ray Systems: Madison, WI, 2006.
(80) Evans, D. F. *J. Chem. Soc.* **1959**, 2003−2005.
(81) Sur, S. K. *J. Magn. Reson.* **1989**, *82*, 169−173.
(82) Frisch, M. J.; Trucks, G. W.; Schlegel, H. B.; Scuseria, G. E.; Robb, M. A.; Cheeseman, J. R.; Scalmani, G.; Braone, V.; Mennucci, B.; Petersson, G. A. et al. *Gaussian 09*, Revision A. 1; Gaussian, Inc.: Wallingford, CT, 2009.

(83) Becke, A. D. *Phys. Rev. A* **1988**, *38*, 3098−3100.
(84) Perdew, J. P. *Phys. Rev. B* **1986**, *33*, 8822−8824.
(85) Hay, P. J.; Wadt, W. R. *J. Chem. Phys.* **1985**, *82*, 299−310.
(86) Roy, L. E.; Hay, P. J.; Martin, R. L. *J. Chem. Theory Comput.* **2008**, *4*, 1029−1031.
(87) Ehlers, A. W.; Bohme, M.; Dapprich, S.; Gobbi, A.; Hollwarth, A.; Jonas, V.; Kohler, K. F.; Stegmann, R.; Veldkamp, A.; Frenking, G. *Chem. Phys. Lett.* **1993**, *208*, 111−114.
(88) Dunning, T. H.; Hay, P. J. In *Modern Theoretical Chemistry*; Schaefer, H. F., Ed.; Plenum: New York, 1976; Vol. 3, pp 1−28.
(89) Glendening, E. D.; Reed, A. E.; Carpenter, J. E. *NBO Version 3.1*.
(90) Hall, M. B. F., R. F. *Inorg. Chem.* **1972**, *11*, 768−779.
(91) Bursten, B. E.; Jensen, J. R.; Fenske, R. F. *J. Chem. Phys.* **1978**, *68*, 3320.
(92) Manson, J.; Webster, C. E.; Perez, L. M.; Hall, M. B. http://www.chem.tamu.edu/jimp2/index.html.